# Enhanced Frequency Stabilization in Interconnected Power Grids with Wind-PV-BESS Using Metaheuristic-tuned Controllers

**Abdelfattah M. Elmoaty[1,*], Ahmed M. Othman[1,2], Mahdi M. Elarini[1]**

[1] *Department of Electrical Power and Machines Engineering, Zagazig University, Egypt*
[2] *Faculty of Electrical Engineering, Centennial College, Toronto, Canada*
[*] Corresponding Author: am.abdelmouty@eng.zu.edu.eg

**Abstract-** This paper suggests an effective controller for frequency regulation of dual-area power networks that are heavily penetrated by renewable energy resources. The purpose of frequency controllers on variable speed wind turbines is to effectively manage the pitch angle and droop controller for frequency support and release the energy contained in spinning masses. Employing an auxiliary controller, solar PV sources equipped with Battery Energy Storage System (BESS) can influentially contribute to the frequency regulation. The Puma Optimizer (PO) is employed to fine-tune the optimal parameters of proportional integral derivative with filter controllers, as well as droop, pitch angle, and auxiliary storage controllers. Integral Time of Absolute Error (ITAE) is proposed as the fitness cost function of frequency deviation in both areas and tie-line power deviation. The superiority of PO is validated by comparing result with benchmarked algorithms such as Genetic Algorithm (GA), Gorilla Troops Optimizer (GTO), Walrus Optimization Algorithm (WaOA), and Hippopotamus Optimizer (HO). It is observed that PO granted lower ITAE by 2.621%, 24.879%, 21.337%, and 43.164% than WaOA, HO, GTO and GA respectively under +20% step load perturbation (+10% at each area). Furthermore, the performance and feasibility are confirmed under random load perturbation and variable weather conditions.
**Keywords** Puma Optimizer; Frequency Regulation; Wind Turbine; Pitch Angle; PIDN Controller.

**List of Abbreviations**

| | | | | | |
|---|---|---|---|---|---|
| AGC | : | Automatic Generation Control | ITAE | : | Integral Time Absolute Error |
| BD | : | Boiler Dynamics | ITSE | | Integral Time Square Error |
| BESS | : | Battery Energy Storage systems | LFC | : | Load Frequency Control |
| BFOA | : | Bacterial Foraging Optimization Algorithm | LJ | : | Luuka-Jaakola |
| CMA-ES | : | Covariance Matrix Adaptation Evolution Strategy | MFF | : | Modified Fitness Function |
| COA | : | Coot Optimization Algorithm | MNUS | : | Minimum Negative Undershoot |
| CSG | : | Conventional Synchronous Generator | MPC | : | Model Predictive Control |
| CTD | : | Communication Time Delay | MPOS | : | Maximum Positive Overshoot |
| DAPS | : | Dual-Area Power System | MWOA | : | Modified Whale Optimization Algorithm |
| DE | : | Differential Evolution | NMS | : | Nelder-Mead Simplex |
| DEG | : | Diesel Engine Generator | OS | : | Over-Shoot |
| DFIG | : | Doubly Fed Induction Generator | PID | : | Proportional Integral Derivative Controller |
| EHO | : | Elephant Herd Optimizer | PIDN | : | Proportional Derivative Controller with Filter |
| ESS | : | Energy Storage System | PLL | : | Phase Locked Loop |
| FA | : | Firefly Algorithm | PV | : | Photovoltaic |
| FC | : | Fuel Cell | PO | : | Puma Optimizer |
| FF | : | Fitness Function | PS | : | Power System |
| FOPID | : | Fractional Order Proportional Integral Derivative Controller | PSO | : | Particle Swarm Optimization |
| GA | : | Genetic Algorithm | RER | : | Renewable Energy Resources |
| GDB | : | Governor Deadband | RLP | : | Random Load Perturbation |
| GOA | : | Grasshopper Optimization Algorithm | SFO | : | Stochastic Fractal Optimizer |

| | | | | | |
|---|---|---|---|---|---|
| GRC | : | Generation Rate Constraint | SHADE | : | Success History-based Adaptation Differential Evolution |
| GTO | : | Gorilla Troops Optimizer | SLP | : | Step Load Perturbation |
| GWO | : | Grey Wolf Optimization | SMC | : | Sliding Model Controller |
| GWO-R | : | Representative-based Grey Wolf Optimization | TID | : | Tilt Integral Derivative Controller |
| HBA | : | Honey Badger Algorithm | US | : | Under-Shoot |
| HO | : | Hippopotamus Optimizer | VSWT | : | Variable Speed Wind Turbine |
| HPSO-GWO | : | Hybrid Particle Swarm Optimization and Grey Wolf Optimization Algorithm | WaOA | : | Walrus Optimization Algorithm |
| HVDC | : | High Voltage Direct Current | WCA | : | Water Cycle Algorithm |
| IMG | : | Isolated Microgrid | WOA | : | Whale Optimization Algorithm |
| ISE | : | Integral Square Error | | | |

## 1. Introduction

Power Systems (PSs) are massive and consist of generating, transmission, and distribution networks, along with the loads dispersed across the whole system. The goal of a PS is to continuously provide individuals with electric power of adequate quality. Electricity consumers fluctuate their loads instantly and randomly; therefore, without a generation-load balancing, electricity cannot be supplied efficiently [1–4]. Load demand-induced fluctuations may have a significant impact on the system's frequency and the tie-line power between the different zones. Frequency deviations outside of the PS's typical range can threaten the system's efficiency, reliability, and safety, resulting in protective system malfunctions, load efficacy interruptions, transmission lines overloads, and equipment defects. Exceptional and acceptable quality in a PS indicates that, irrespective of the fluctuations that occur in loads arbitrarily, frequency and voltage must be consistent and remain at the required values. Eliminating the influence of load variation and maintaining the frequency and voltage levels consistently necessitates managing the system [5–8].

The issues of frequency control and voltage control can be distinguished from one another, even though active and reactive powers have a compound influence on both. Frequency generally relies on active power, whereas voltage relies on reactive power; consequently, PS control can be split into two separate problems [9–11].

The Load Frequency Control (LFC), which stands for active power and frequency control, is essential to the quality and reliability of PSs. In the event of parametric uncertainties and interruptions in the external loads, LFC ensures that the PS operates efficiently and manages the frequency and tie-line power deviations to maintain them at zero. Sudden perturbations in load on traditional electricity networks are mitigated by the energy stored in conventional synchronous generators (CSG) spinning masses, till primary controllers operate through speed governors and secondary LFC loop [12–14]. Currently, the growing scale and intricacy of PSs, coupled with the limitations of conventional units, elevated running expenses, fossil fuels depletion, ecological restrictions, the advancement of Renewable Energy Resources (RER), as well as the adoption of novel ideas like smart grids, have all contributed to the complexity of today's modern PSs. The aforementioned causes have a direct impact on the PSs' performance, stability, and security. In addition, they have necessitated the implementation of LFC in contemporary PSs greater than ever before. Frequency response amelioration can be separated into three defined divisions: primary, secondary, and tertiary control. The governor droop regularly carries out the core of frequency amelioration, leading to repeated reported discrepancies in steady state readings. Before the under/over frequency relays work, the frequency fluctuations are registered by means of the primary frequency control loop. Furthermore, a clean secondary frequency control, also denoted as Automatic generation control (AGC), is required to maintain the balance between the load demand and the generated power. Therefore, the frequency is kept constant or at least within the desired range [15–17]. The hierarchical architecture of the LFC approach is represented in Figure 1.

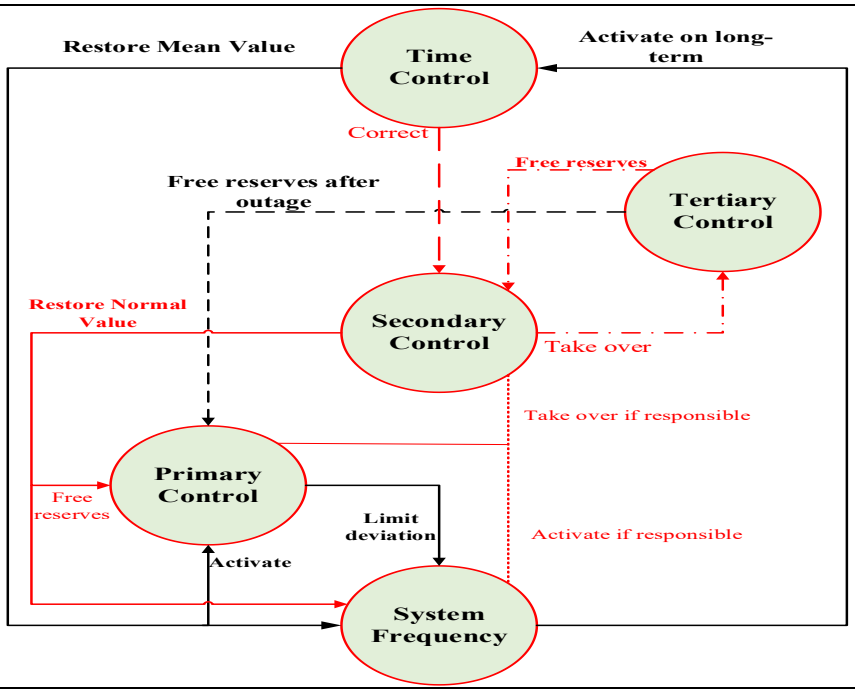



**Figure 1.** Hierarchical architecture of LFC strategy

Without a doubt, switching from CSGs to RERs will result in less system inertial energy being available, which could lead to more frequency challenges [18–20]. As a result, minimum frequency variations must be linked to the RERs' network penetration. However, because of the fluctuations in generation and load, the PS's frequency is frequently beyond its acceptable range [21,22]. Various methods of control are used for this objective, including integer order Proportional Integral Derivative (PID) controllers, fractional order PID (FOPID) controllers, Tilt Integral Derivative (TID) controllers, and cascaded or dual-stage controllers. In addition, contemporary control strategies that incorporate the finest control methods, such as adaptive control, Model Predictive Control (MPC), and Sliding Mode Control (SMC), are also employed. Fuzzy logic control, artificial neural networks, and adaptive neuro fuzzy inference systems are among the intelligent control technologies explored. Moreover, robust approaches, including H∞, data-driven control, and virtual inertia control devices based on energy-efficient Energy Storage Systems (ESSs), have been researched to improve frequency. Furthermore, numerous studies have been conducted on the contribution of demand response programs, electric vehicles, and flexible alternating current transmission systems [23–25].

The authors in [26] suggested Modified Whale Optimization Algorithm (MWOA) for optimizing the parameters of the LFC of dual-area interconnected PS. The employed controllers were PID and PID with filter (PIDN) controllers. The performance of the two controllers was analyzed and compared in several aspects. In [27], Guha D, et al. proposed a dual-area thermal system with HVDC tie-link. Furthermore, system non-linearities such as Governor Deadband (GDB), Generation Rate Constraint (GRC), Boiler Dynamics (BD), and Communication Time Delay (CTD) were considered to justify the frequency measurement and Phase Locked Loop (PLL) effects on PS stability. Besides that, a supplementary power modulation controller was analyzed and considered with PLL and HVDC link dynamics in order to improve system performance. In addition, a WOA-based PID controller was implemented for LFC of the proposed system under different system disturbances. Besides that, [28] proposed a PID controller for AGC of two and three areas interconnected PSs. Improved Stochastic Fractal Search Algorithm (ISFS) based PID controller was compared with Bacterial Foraging Optimization Algorithm (BFOA), hybrid BFOA and Particle Swarm Optimization (HBFOA-PSO) based PI controllers, as well as Teaching Learning based Optimization (TLBO) based PID controller to validate its potency.

Additionally, the authors in [29] proposed a novel cascaded controller comprised of Proportional Integral and One plus Integral Derivative (PI-(1+ID)) for a single-area Isolated Microgrid (IMG). The IMG comprises generation from wind turbines, solar thermal, biodiesel power generators, as well as solid oxide fuel cells. The controller's parameters were tuned using the Butterfly Algorithm (BFA). To evaluate the proposed technique's efficacy, a comparison with several controllers such as PI, PID, and PI-(1+ID) controllers optimized by Particle Swarm Optimizer (PSO) and Grasshopper Optimization Algorithm (GOA) is conducted. Besides that, the authors

in [30] presented a Quasi-Oppositional African Vulture Optimization Algorithm (QOAVOA) for tuning the hybrid FOPIDN and FOPI controllers connected in parallel. The optimized controller was employed for LFC of dual-area interconnected PS with/without RER penetrations.

Moreover, like traditional turbines with CSGs, Variable Speed Wind Turbines (VSWT) can offer frequency adaptations through stored energy in their rotors. Furthermore, it is found that the response time of steam, gas, or hydro turbines is slower than that of a VSWT led with a Doubly Fed Induction Generator (DFIG) employing the reference torque command. The authors demonstrated how a wind turbine with a frequency-controlled pitch controller in addition to droop characteristics significantly improves the system frequency responsiveness in a small hydro system that is 50% powered by wind [31,32].

A fuzzy-based TID controller was suggested for the LFC of multi-area PS. The parameters were optimized using the Artificial Hummingbird Algorithm (AHA). GRC was considered in the system. The performance of the proposed technique was proven to be superior by comparison with GOA and the bird swarm algorithm. Dish-stirling thermal and wind turbine systems were integrated and analyzed in the proposed system. A conventional and accurate model of HVDC tie-link was also introduced and compared with the AC tie-link in system dynamics. The controller's performance was validated by a comparison with classic TID and PID controllers [33]. In addition, MPC is a complex control approach that has achieved acceptance in LFC applications. In [34], MPC was suggested in dual-area hybrid PS to control the charging and discharging states of ESSs. The proposed strategy was selected to minimize the frequency deviations to zero in the presence of system disturbances. Moreover, MPC can be considered as an advanced strategy in case of faults and physical detachment. Centralized, decentralized, and distributed MPC controllers based on a free fault-tolerant model were presented in [35] to regulate frequency deviations in case of tie-line power disconnections of the four-area PS. Additionally, further works introducing LFC are presented and compared with the proposed methodology in Table 1.

**Table 1** Comparison between previously published and proposed work

| NO. | System Type | No. of Areas | Sources | ESSs | Controller | Optimization Algorithm | Fitness Function | Remarks |
|---|---|---|---|---|---|---|---|---|
| [18] | Hybrid | 2 | Thermal, Hydro, PV, VSWT | BESS | PID | SFO | ITAE | -Real wind speed and sun irradiation data are extracted from Zafarana, Egypt.<br>-Studied under SLP and RLP.<br>-SSO is compared with GA, where both presented the same results in OS, US, and settling time.<br>-Authors didn't consider the effect of RERs on system inertia and regulation constants. |

| | | | | | | | | |
|---|---|---|---|---|---|---|---|---|
| [36] | IMG | 1 | PV, DEG, FC | BESS | PID | hPSO-GWO | ITSE | -Studied different cases of SLP.<br>-Provided better results than unoptimized PID, GWO: PID, and PSO: PID controllers.<br>-Real-time implementation is performed using the dSpace 1104 simulator. |
| [37] | Conventional | 2 | Thermal, Hydro, and Gas | ___ | PID | DE/FA | ITAE | -Studied under continuous SLP.<br>-Real-time implementation is performed using the OPAL-RT simulator.<br>-FA had better results than DE.<br>-Studied the effect of HVDC tie-link. |
| [38] | Conventional | 2 | Thermal | ___ | PIDN | GWO-R | MFF | -R-method assisted in getting the weights of MFF.<br>-Studied several cases of SLPs.<br>-Compared with DE, EHO, NMS, JAYA, LJ, CMA-ES, SHADE, and GWO techniques.<br>-Presented statistical analysis to prove the robustness. |

| | | | | | | | | |
|---|---|---|---|---|---|---|---|---|
| [39] | Hybrid | 2 | Thermal, Hydro, PV, VSWT | BESS | PID | COA | ISE | -Real wind speed and sun irradiation data are extracted from Zafarana, Egypt.<br>-Studied under SLP and RLP.<br>-COA is compared with PSO, WCA, and HBA, where it presented better results in OS and US .<br>-Didn't consider the effect of RERs on regulation and frequency bias constants. |
| **Proposed** | Hybrid | 2 | Thermal, Hydro, PV, VSWT | BESS | PIDN | PO | ITAE | -Real wind speed and sun irradiation data are extracted from Zafarana, Egypt.<br>-Studied under SLP and RLP.<br>- PO is compared with HO, GA, GTO, and WaOA.<br>-Consider the effect of RERs on system inertia and regulation constants, unlike [18,39] |

Assessing the literature of the subject indicated that the multi-resource, multi-area systems in the presence of RERs have been among the most significant issues in recent years. Although these studies have sought to provide new ideas in this sector, the absence of a study that can consider all these resources comprehensively, is may still be noticed in the literature. Accordingly, the authors of this paper are encouraged to apply a new nature-based meta-heuristic algorithm, called Puma Optimizer (PO). The proposed algorithm was employed in tuning the PIDN controller's parameters, as well as pitch angle and droop controllers' gain and time constant of the washout filter of the Battery Energy Storage System (BESS). Based on the clarifications, the most significant contributions and aspects of this study are: (i) Proposing a complete model of LFC by considering diverse

sources, including RERs, ESSs, etc. (ii) Optimizing PIDN controllers, wind turbine generator droop and pitch angle controllers with PO. (iii) Analyzing and studying the dual-zone model with RERs and comparing results with other methods in the time domain. (iv) Studying the system under variable weather conditions and random load perturbations.

The remainder of this article is structured as follows: Section 2 introduces the mathematical models of the proposed resources and system. Besides, section 3 elaborated on the inspiration and procedures of the proposed PO. In Section 4, the results of simulations, numerical and comparative analyses are presented. Finally, in Section 5, a general conclusion and summary of the paper's outcome are presented.

## 2. System overview and modelling

As depicted in Figure 2, the intended system is a dual-area hybrid PS (DAPS). The system comprises traditional units such as steam and hydro turbine power plants as well as RERs and ESSs. Area 1 is made up of 50% VSWT and 50% traditional steam turbine power plant. On the other hand, Area 2 is made up of 20% Photovoltaic (PV) solar energy as well as 80% hydro turbine power plant. The succeeding subsections provide a full and complete overview of the system components along with control signals.

### *2.1. Wind turbine model*

This work utilizes the dynamical model of VSWT with a 3.6 MW rating power. Its parameters are provided in Table 2. Regarding frequency stability assessments, the rapid reaction of switching transients in the converter and electromagnetic transients in generator windings is often disregarded in favor of focusing on the slower dynamics of the turbine and rotor [21,40]. The block diagram of VSWT is demonstrated in Figures 3, 4, and 5. The PI controller depicted in Figure 3 produces an output torque signal ($T_{cmd}$) that is reliant upon the deviation in wind turbine speed. This model was chosen to determine how the planned DAPS would behave dynamically in the event of power perturbations. The output mechanical power that a wind turbine can produce is given by Eq. (1)

$$P_m = 0.5 * \rho * A_{wt} * V_w^3 * C_p(\beta, \lambda) \tag{1}$$

where $\rho$ is the air density in $kg/m^3$, $A_{wt}$ is the Swept area in $m^2$, and $V_w$ is the wind speed in m/s (presumed 11m/s). The power coefficient $c_p$ is given by Eq. (2) as follows:

$$C_p(\beta, \lambda) = \sum_{i=0}^{4} \sum_{j=0}^{4} \alpha_{i,j} * \beta^i * \lambda^j \tag{2}$$

where β is the pitch angle, $\alpha_{i,j}$ coefficients are given in [40], and $\lambda$ is the ratio of rotor blade tip speed and wind speed as shown in Eq. (3)

$$\lambda = \frac{V_{tip}}{V_w} = \frac{K_b * \omega_{wt}}{V_W} \tag{3}$$

where $V_{tip}$ is the rotor blade tip speed, $\omega_{wt}$ is the wind turbine rotor speed, and $K_b$ is a fixed constant and represents the relationship between blade tip speed and turbine rotor speed. Applying a cubic curve fitting, the reference speed of the wind turbine for maximum power point tracking (MPPT) can be found by Eq. (4).

$$\omega_{wt,ref} = 1.6 * P_e^3 - 2.7 * P_e^2 + 2.3 * P_e + 0.45 \tag{4}$$

where $\omega_{wt,ref}$ is the reference speed of the wind turbine and $P_e$ is the output electrical power. The upper and lower constraints of wind turbine speed are 1.2 and 0.7 pu, respectively.

The droop controller developed in Figure 5 functions similarly to the CSG's droop controller. The steady state value of the power signal $P_{droop}$ will be 0 if the VSWT is situated in a region with AGC committed to traditional units. As a result, $P_{droop}$, a transient signal whose intensity is proportionate to the frequency deviation, acts to either accelerate or decelerate the rotor when the frequency variation is − or +, respectively. The power signal $P_{droop}$ is dependent on frequency deviation of area-I $\Delta F_1$ for adjusting the VSWT's output power concerning frequency changes.

Moreover, the purpose of the pitch angle controller is to prevent the turbine from producing power that exceeds the rated capacity of the generator when there are high wind speeds. This objective is accomplished by using the control circuit demonstrated in Figure 5. The pitch angle, denoted as $\beta_{ref}$, is the specific angle needed to control the rotor speed and maintain it at its predetermined reference value. In the usual wind speed range, $\beta_{ref}$ is set to zero. However, for wind speeds above the normal range, $\beta_{ref}$ is set to a number larger than zero. The offset angle $\beta_f$ is an extra angle that is added to limit wind turbine output when there are positive frequency variations [18]. Furthermore, it may be used to harness additional wind energy in the event of

negative frequency variations and within elevated wind speed ranges. The subsequent usage is restricted by the generator's transient overloading capacity.

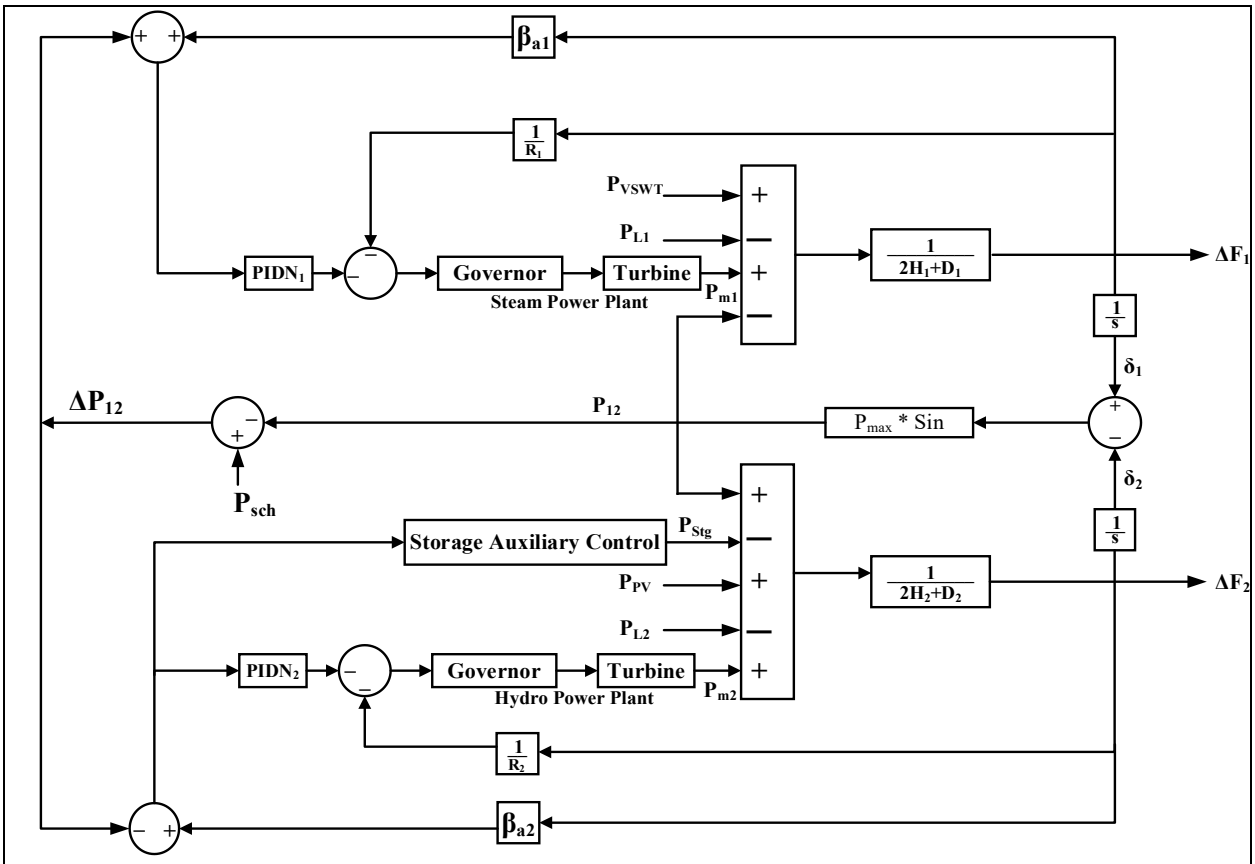



**Figure 2.** DAPS with RERs and ESSs penetration

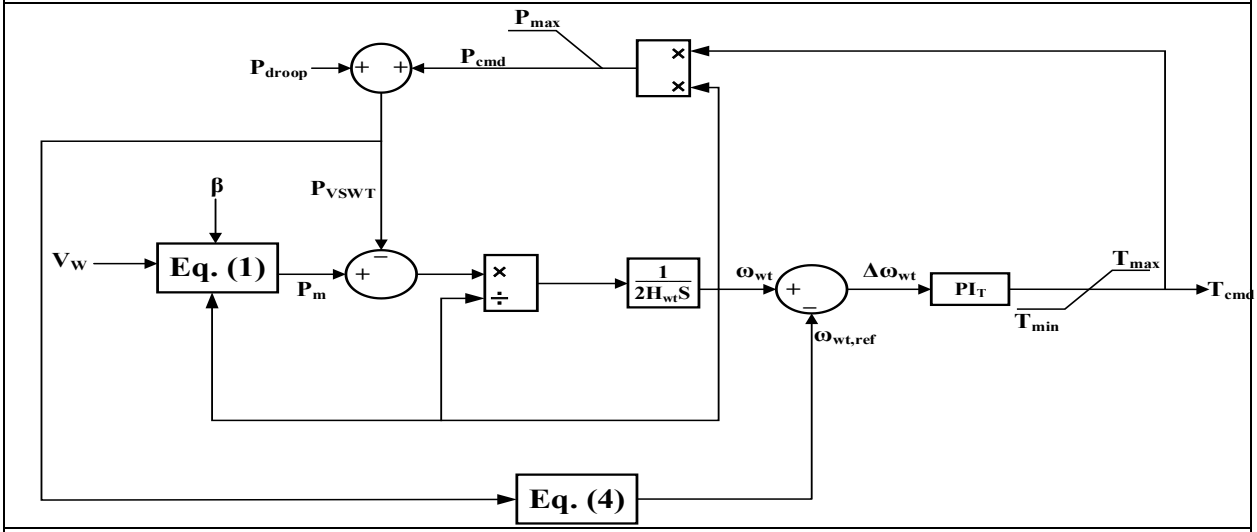



**Figure 3.** The dynamical model of VSWT

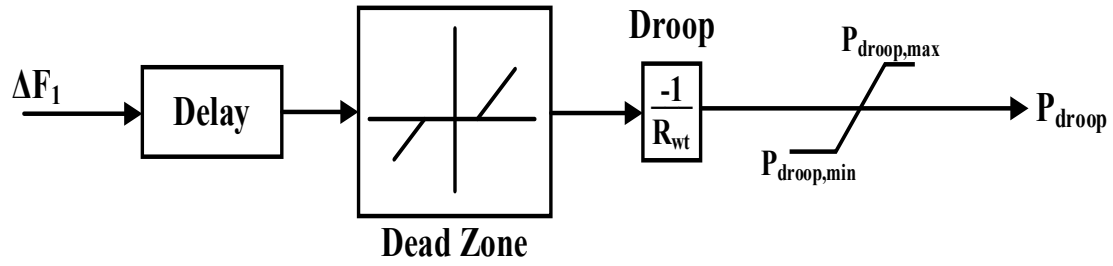



**Figure 4.** The Frequency droop controller

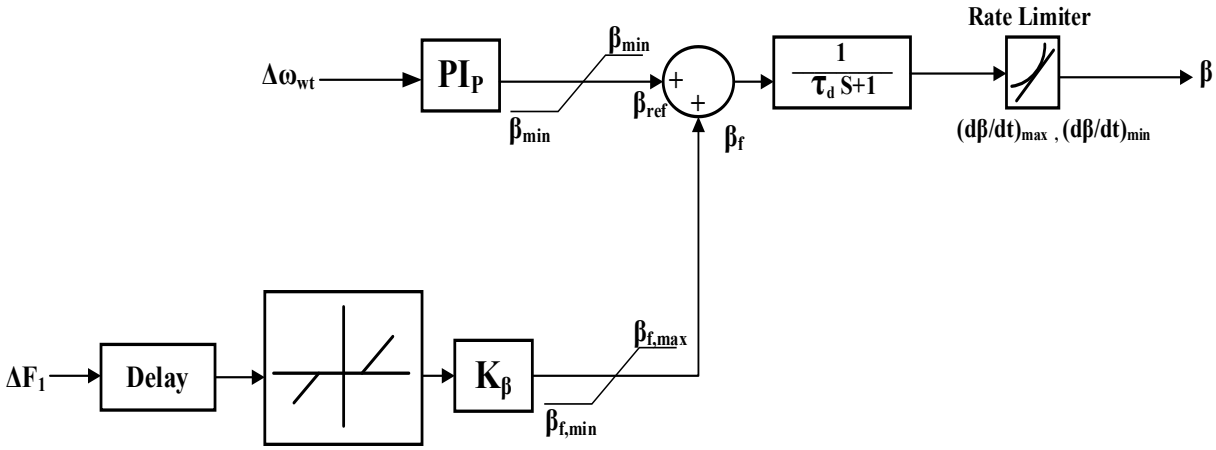



**Figure 5.** The pitch angle controller

### *2.2. PV model*

The PV module's mathematical representation is provided in Eqs. (5)-(10) [41,42]. Table 2 contains data collected from [42] for simulating the PV system's electrical properties. The parallel resistance varies with solar irradiation [43,44], as seen in equation Eq. (9). On the contrary, the series resistance remains constant regardless of irradiation under both operational and normal test circumstances [43,44].

$$V_t = \frac{K_{Bz} * T}{Q_e} \tag{5}$$

$$I_{ph} = \left(\frac{G}{G_{ref}}\right)\left(I_{phn} + K_i\left(T - T_{ref}\right)\right) \tag{6}$$

$$I_0 = I_{sc}\left(\frac{G}{G_{ref}}\right)\left(\frac{T}{T_{ref}}\right)^3 e^{\left(1-\frac{V_{oc}}{MV_t}\right)} \tag{7}$$

$$I_{PV} = I_{ph} - \left(\frac{I_{PV}R_s + V_{PV}}{R_p}\right) - I_0\left(e^{\left(\frac{I_{PV}R_S + V_{PV}}{MV_t}\right)} - 1\right) \tag{8}$$

$$R_p = R_{ps}\left(\frac{G}{G_{ref}}\right) \tag{9}$$

$$P_{PV} = V_{PV}I_{PV} \tag{10}$$

where the PV thermal voltage is $V_t$, the PV temperature is T, the Boltzmann constant is $K_{Bz}$, the electron charge is $Q_e$, $T_{ref}$ and $G_{ref}$ are temperature and irradiance at standard circumstances, respectively, and the actual irradiance and temperature are G and T, respectively. In addition, $I_{phn}$ and $I_{ph}$ are the corresponding light-generated current at standard circumstances and actual temperature, respectively. The short-circuit current temperature coefficient is denoted by $K_i$. The short-circuit current and the reverse saturation diode current are expressed by $I_{sc}$ and $I_0$, respectively. The open circuit voltage is expressed by $V_{oc}$ and M represents the diode ideality factor. $R_p$, $R_S$, and $R_{ps}$ represent the shunt, the series, and the standard condition shunt resistances, respectively. Besides that, the PV output current, voltage, and power are denoted by $I_{PV}$, $V_{PV}$, and $P_{PV}$ respectively.

Employing an Artificial Neural Network (ANN) based MPPT technique, the PV output voltage is assessed. Following multiple attempts, it is decided to utilize one hidden layer with fifteen hidden neurons with tan-sigmoid activation functions and one output layer neuron with a linear activation function. The ANN is trained offline in order to determine the voltage at MPP in accordance with solar irradiance and temperature levels [45]. Once the voltage at MPP has been determined, Eqs. (5)-(10) are employed to compute the output current and maximum achievable power. The PV system's output power is then added to the area's supplied electricity, as illustrated in Figure 2.

### *2.3 Traditional units modelling*

The suggested DAPS includes steam and hydropower units. The mathematical model of the steam turbine and generator are presented in Eqs. (11)–(13). According to [46], the steam turbine representation is predicated on a single reheat phase.

| | | |
|---|---|---|
| Turbine model | $\frac{F_{HP}T_{RH}\,S+1}{(T_{RH}S+1)(T_{CH}S+1)}$ | (11) |
| Governor model | $\frac{1}{T_G S+1}$ | (12) |
| Generator Model | $\frac{1}{2\,H_1 S+D_1}$ | (13) |

where $T_{CH}$ and $T_{RH}$ and are the main inlet valve and reheater time constants, and $F_{HP}$ represents the fraction power generated by the high-pressure turbine. The time constant $T_G$ represents the governor time lag. The generator model is described by the swing equation where $H_1$ and $D_1$ represent its inertia and load-damping constant, respectively.

Furthermore, the transfer function of hydro power plant's turbine, governor, and generator are described by Eqs. (14)-(16). The mathematical representation of hydro turbine is a non-minimum phase system that accounts for the changes in output power owing to its gate opening. In contrast to a steam turbine governor, a hydro turbine governor needs an extra transient droop and an extensive restoring period to restrict gate movement until water flow and output power are given enough time to catch up [46].

| | | |
|---|---|---|
| Turbine model | $\frac{-T_W S+1}{0.5T_W S+1}$ | (14) |
| Governor model | $\frac{T_R S+1}{(T_{GH}S+1)\left(\left(\frac{R_{Td}}{R_{Pd}}\right)T_R\,S+1\right)}$ | (15) |
| Generator Model | $\frac{1}{2\,H_2 S+D_2}$ | (16) |

Where $T_W$ and $T_R$ are the water starting time and reset time, respectively. $T_{GH}$ represents a time constant expressing the delay in the governor response. The generator model is described by the swing equation where $H_2$ and $D_2$ represent its inertia and load-damping constant, respectively.

### *2.4 Energy storage controller*

When compared to VSWT intrinsic control, storage devices respond more quickly, so adding an auxiliary controller to batteries allows them to temporarily participate in frequency control. Figure 6 displays the block diagram of the auxiliary controller. To supply a transitory signal at brief intervals, a washout circuit is employed. Because of the limitations on the depth of discharge, an output signal limiter is utilized in addition to the maximum charging/discharging rates.

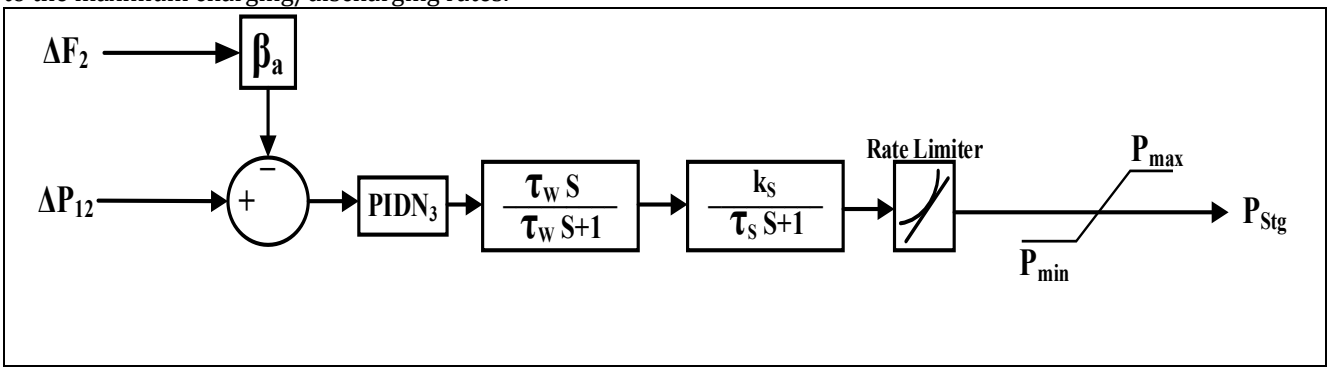


**Figure 6.** Energy storage auxiliary controller

### *2.5 Tie-line power and load models*

Frequency control studies utilize composite load models which have two components: a fixed component that is frequency invariant and a frequency-dependent part that is expressed in terms of load damping constant (D) as [46]:

$$P_{Load} = P_L + D \cdot \Delta F \quad (17)$$

Therefore, the tie-line power and its small deviation are illustrated as

$$P_{12}\ or\ P_{tie} = P_{max} \sin(\delta_1 - \delta_2) \quad (18)$$

$$\Delta P_{12} = P_{Sch} - P_{12} \quad (19)$$

where $P_{12}\ or\ P_{tie}$ represents the tie-line power. The maximum and scheduled tie-line power levels are 1.0 and 0.2 pu, respectively.

**Table 2** Proposed power system parameters

| **Area-I** | | | | **Area-II** | | |
|---|---|---|---|---|---|---|
| **Parameter** | **Value** | **Unit** | | **Parameter** | **Value** | **Unit** |
| $H_1^*$ | 3 | $S$ | | $H_2^*$ | 3 | $S$ |
| $D_2$ | 1 | $pu$ | | $D_2$ | 1 | $pu$ |
| $R_1^*$ | 0.05 | $pu$ | | $R_2^*$ | 0.05 | $pu$ |
| $\beta_{a1}^*$ | 21 | $pu$ | | $\beta_{a2}^*$ | 21 | $pu$ |
| **Steam power plant** | | | | **Hydro power plant** | | |
| $F_{HP}$ | 0.3 | $__$ | | $T_W$ | 1 | $s$ |
| $T_{RH}$ | 7 | $s$ | | $T_R$ | 0.513 | $s$ |
| $T_{CH}$ | 0.3 | $s$ | | $T_{GH}$ | 48.7 | $s$ |
| $T_G$ | 0.2 | $s$ | | $R_T\ /R_P$ | 19.493 | $__$ |
| **VSWT on its base** | | | | **PV (per module)** | | |
| $H_{wt}$ | 5.74 | $s$ | | $I_{phn}$ | 8.2527 | $A$ |
| $PI_T$ | $K_p = 3$ | $pu$ | | $R_s$ | 0.134 | $\Omega$ |
| | $K_I = 0.3$ | | | $R_{ps}$ | 134.48 | $\Omega$ |
| $P_{max}$ | 3.6 | $MW$ | | $M$ | 1.282 | $__$ |
| $T_{max}$ | 0.833 | $pu$ | | $G_{ref}$ | 1000 | $W/m^2$ |
| $T_{min}$ | 0 | $pu$ | | $T_{ref}$ | 25 | $°C$ |
| **Droop and Pitch controllers** | | | | $K_i$ | 0.037 | $\%/°C$ |
| $Delay$ | 100 | $ms$ | | $V_{oc}$ | 33.12 | $V$ |
| $Deadzone$ | 0.001 | $pu$ | | $I_{sc}$ | 8.2 | $A$ |
| $P_{droop,max}$ | 0.2 | $pu$ | | $V_{MPP}$ | 27.28 | $V$ |
| $P_{droop,min}$ | $-0.2$ | $pu$ | | $I_{MPP}$ | 7.5 | $A$ |
| $PI_P$ | $K_P = 50$ | $pu$ | | $P_{MPP}$ | 204.6 | $W$ |
| | $K_I = 0.3$ | | | **Auxiliary storage controller** | | |
| $\tau_d$ | 0.3 | $s$ | | $k_s$ | 0.98 | $pu$ |
| $\beta_{max}$ | 27 | $Degree$ | | $\tau_s$ | 0.03 | $s$ |
| $\beta_{min}$ | 0 | $Degree$ | | $P_{max}$ | 0.1 | $pu$ |
| $\left(\frac{d\beta}{dt}\right)_{max}$ | 10 | $Degree/s$ | | $P_{min}$ | $-0.1$ | $pu$ |
| $\left(\frac{d\beta}{dt}\right)_{min}$ | $-10$ | $Degree/s$ | | $\left(\frac{dP}{dt}\right)_{max}$ | 0.1 | $pu/s$ |
| $\beta_{f,max}$ | 10 | $Degree$ | | $\left(\frac{dP}{dt}\right)_{min}$ | $-0.1$ | $pu/s$ |
| $\beta_{f,min}$ | $-10$ | $Degree$ | | | | |

* denotes that values are with 0% RERs penetration

## 3. Puma optimizer mathematical representation

PO is a newly developed meta-heuristic algorithm presented by Benyamin Abdollahzadeh et al in [47,48] based on the natural behavior of pumas. The PO algorithm employs a novel purposeful approach to alter the phases

of exploration and exploitation, which was the first time it had been disclosed. Throughout each stage of exploration, distinct methodologies have been employed to enhance optimization operations. Plus, two distinct methods have been implemented, drawing inspiration from the natural behavior of pumas. Each solution underwent either an exploitation or exploration phase in each iteration, utilizing the phase change mechanism. The decision about which of these phases is planned and intelligent. Following this, mathematical formulas and equations are provided to illustrate the optimization processes conducted by PO.

### *3.1. Phase change mechanism*

The phase change mechanism in the suggested technique is a sort of heuristic selecting method that uses two aspects of disparity and escalation. This is an algorithm for performing reward and penalty operations for grading. Plus, it also draws inspiration from pumas' intellect. It takes a pair of strategies: the first is that pumas attempt to simultaneously look and ambush for prey by exploring new territory since they lack the necessary energy and experience.

#### *3.1.1. Unexperienced phase*

Both exploration and exploitation phases are performed in the first three iterations until the phase change stage's startup is completed. It can be performed using two functions as presented in Eqs. (20)-(21) where the "stage" term is related to either the exploration or exploitation phases.

$$f_{1\ stage} = PF_1 \cdot \left(\frac{Seq^1{}_{Cost,Stage}}{Seq_{Time}}\right) \tag{20}$$

$$f_{2\ stage} = PF_2 \cdot \left(\frac{\sum_{i=1}^{3} Seq^i{}_{Cost,Stage}}{\sum_{i=1}^{3} Seq^i{}_{Time}}\right) \tag{21}$$

where $Seq^i{}_{Time}$ are constant value variables. The coefficients, PF1 and PF2, which are used to rank each of the $f_1$ and $f_2$ functions, have preset settings between 0 and 1, and must be defined before the optimization process. Plus, $Seq_{Cost,Stage}$ , which are variable values related to the phase of exploration and exploitation, can be calculated as follows in Eqs. (22)-(24).

$$Seq^1_{Cost,Stage} = \left|Cost^{Initial}_{Best} - Cost^1_{Stage}\right| \tag{22}$$

$$Seq^2_{Cost,Stage} = \left|Cost^2_{Stage} - Cost^1_{Stage}\right| \tag{23}$$

$$Seq^3_{Cost,Stage} = \left|Cost^3_{Best} - Cost^2_{Stage}\right| \tag{24}$$

where $Cost^i_{Best}$ for i=1,2,3 are the fitness function (FF) of the best solution obtained in each phases of exploitation or exploration and $Cost^{Initial}_{Best}$ is the FF of the starting solution generated during the initialization stage. Afterwards, there is just one choice made for the exploration and exploitation stages. Due to the positive experiences of other Pumas, both aspects of the exploitation and exploration stages are computed to select one of the two phases utilizing Eq. (25).

$$Score_{Stage} = \left(PF_1 \cdot f1_{Stage} + PF_2 \cdot f2_{Stage}\right) \tag{25}$$

using $Score_{Stage}$ of both phases, if $\text{Score}_{\text{Explore}} > \text{Score}_{\text{Exploit}}$, enters the exploration phase or else enters the exploration stage.

#### *3.1.2. Experienced phase*

After finishing the first three iterations, pumas can choose only one phase for the optimization process as they have an appropriate level of experience to determine whether to alter the phases. Three functions are employed for scoring during this phase. The first function $f_1$ highlights the rise element and determines which of the exploration and exploitation phases has been chosen and executed perfectly than the other. $f_1$ can be calculated utilizing Eq. (26).

$$f_{1Iter}^{Stage} = PF_1 \cdot \left|\frac{Cost_{old}^{Stage} - Cost_{new}^{Stage}}{T_{Iter}^{Stage}}\right| \tag{26}$$

where $f_{1_t}^{Stage}$ refers to either exploration or exploitation phases first function values. Iter refers to the current iteration number. $Cost_{old}^{Stage}$ refers to the FF of the previous best solution before advancement in the present selection. $Cost_{new}^{Stage}$ refers to the FF of the new best solution attained after advancement in the current choice. $T_{Iter}^{Stage}$ are the quantity of unaltered iterations between the present choice to the prior choice.

Above that, the resonance component can be emphasized and a phase with better performance than the other selected phase using the second function $f_2$. Sequentially, appropriate executions are assessed and checked in order to aid the exploitation phase in its decision-making process. $f_2$ can be calculated utilizing Eq. (27).

$$f_{2_t}^{Stage} = PF_2 \cdot \left| \frac{\sum_{i=1}^{3} \left( Cost_{old,i}^{Stage} - Cost_{new,i}^{Stage} \right)}{\sum_{i=1}^{3} T_{t,i}^{Stage}} \right| \quad (27)$$

where $f_{2_t}^{Stage}$ refers to either exploration or exploitation phases second function. For i=1:3 , $Cost_{old,i}^{Stage}$ represents the FF of best solution before advancement in the current, previous and the two previous choices respectively in exploration and exploitation stages. $Cost_{new,i}^{Stage}$ refers to the FF of the best solution attained after advancement in the current, previous and the two previous choices respectively. $T_{t,i}^{Stage}$ refers to the number of unaltered iterations in each phase of exploration and exploitation between the present and previous choice for i=1, between the one previous and two previous choices for i=2 and between the three previous and the two previous choices for i=3.

Furthermore, the diversity component is prioritized in the selection process using the third function $f_3$. That allows for the possibility of selecting a phase that was not chosen in previous iterations. This is important since selecting just one phase might result in being stuck in a local optimum solution. $f_3$ is calculated using Eq. (28).

$$f_{3_t}^{Stage} = \begin{cases} f_{3_t}^{Stage} = 0 & if\ selected \\ f_{3_t}^{Stage} + PF_3 & otherwise \end{cases} \quad (28)$$

where $f_{3_t}^{Stage}$ is related to the third function referred to either exploration or exploitation stages. Based on Eq. (28), if one of the phases is not chosen, he third function value will be raised by the parameter $PF_3$ or else it going to fall to zero. The parameter $PF_3$ is similar to $PF_1$ $and$ $PF_2$ which isa user configurable parameter that must be assigned before the optimization process with a value between 0 and 1. When the PF3 parameter value is near to 1, phases with low scores have a greater possibility of selection. On the other hand, as the value drops, the likelihood of selection minimizes. Additionally, employing Eq. (29), the final FF of each stage is evaluated.

$$F_t^{Stage} = \left( \alpha_t^{Stage} \cdot \left( f_{1_t^{Stage}} \right) \right) + \left( \alpha_t^{Stage} \cdot \left( f_{2_t^{Stage}} \right) \right) + \left( \delta_t^{Stage} \cdot \left( lc \cdot f_{1_t^{Stage}} \right) \right) \quad (29)$$

$$lc = \{ \{ |Cost_{old} - Cost_{new}| \}^{Exploitation} , \{ |Cost_{old} - Cost_{new}| \}^{Exploration} \} , o \notin lc \quad (30)$$

$$\alpha_t^{explore,\ exploit} = \begin{cases} \alpha^{exploit} = 0.99, \alpha^{explore} = [\alpha^{explore} - 0.01, 0.01] & if\ F^{exploit} > F^{explore} \\ \alpha^{explore} = 0.99, \alpha^{exploit} = [\alpha^{exploit} - 0.01, 0.01] & otherwise \end{cases} \quad (31)$$

$$\delta_t^{Stage} = 1 - \alpha_t^{Stage} \quad (32)$$

During the search process, parameters $\alpha$ and $\delta$ are changeable based on the findings of the exploration and exploitation phases. Diversity is emphasized; otherwise, the emphasized diversity component is lowered, and if the value of parameter $\alpha$ is near to 1, the resonance component is favored. The parameter $\alpha$ can be determined as shown in Eq. (31). In addition, *lc* represents a collection of FF differences from the advancements attained from both exploration and exploitation stages as illustrated in Eq. (30). That involves a collection of quantities other than zero ($lc \notin 0$).

### *3.2. Exploration*

The overall exploration process is shown in the pseudo-code in Algorithm-I using the set of Eqs. (33)-(38).

$$Z_{i,G} = \begin{cases} R_{dim} \cdot (Ub - Lb) + Lb \\ X_{a,G} + G \cdot \left( X_{a,G} - X_{b,G} \right) + G \cdot \left( \left( \left( X_{a,G} - X_{b,G} \right) - \left( X_{c,G} - X_{d,G} \right) \right) + \left( \left( X_{c,G} - X_{d,G} \right) - \left( X_{e,G} - X_{f,G} \right) \right) \right) \end{cases} \quad (33)$$

$$G = 2 \cdot rand_2 - 1 \quad (34)$$

$$X_{new} = \begin{cases} Z_{i,G} & If\ j = j_{rand}\ or\ rand_3 \le U \\ X_{a,G} & Oherwise \end{cases} \quad (35)$$

$$NC = 1 - U \quad (36)$$

$$p = \frac{N}{N_{pop}} \quad (37)$$

$$X_{a,G} = X_{new} \quad if\ X_{i,new} < X_{a,G} \quad (38)$$

**Algorithm I** Pseudo-code of the PO exploration phase

Sort ascending population
Calculate p
for (each Puma ($X_i$)) do
    Select four solutions randomly
    Calculate the new vector by Eq. (33).
    Check the boundary of the new vector position
    Update the current solution by Eq. (35).
    Calculate the cost of the updated solution
    if NewX$_i$$Cost$ $< X_i Cost$
        $X_i = NewX_i$
    else
        U = U + p ;
    end
end

### *3.3. Exploitation*

The PO algorithm uses two distinct operators in the exploitation step to enhance the solutions; these two processes are based on the two hunting habits of pumas: sprinting and ambush hunting.

The PO algorithm uses two distinct operators in the exploitation step to enhance the solutions; these two processes are based on the two hunting habits of pumas: sprinting and ambush hunting. In the wild, pumas attempt to ambush their prey by hiding behind shrubs, trees, or rocks. It can run after its target in some situations. This attitude is simulated as shown in Eq. (39). The full process is illustrated in its pseudo-code in Algorithm-II employing Eqs. (39)-(45)

$$\mathrm{X}_{\mathrm{new}} = \begin{cases} \dfrac{\left(\dfrac{\mathrm{mean}(\mathrm{Sol}_{\mathrm{total}})}{\mathrm{N}_{\mathrm{Pop}}}\right)\cdot \mathrm{X}_1^{\mathrm{r}} - (-1)^{\beta}\times \mathrm{X}_{\mathrm{i}}}{1+(\alpha\cdot \mathrm{rand}_5)} & \text{If } \mathrm{rand}_4 \geq 0.5 \\ \mathrm{X}_{\mathrm{new}} = \mathrm{Puma}_{\mathrm{male}} + (2\cdot \mathrm{rand}_7)\cdot \exp(\mathrm{randn}_1)\cdot \mathrm{X}_2^{\mathrm{r}} - \mathrm{X}_{\mathrm{i}} & \text{If } \mathrm{rand}_6 \geq \mathrm{L} \\ (2\cdot \mathrm{rand}_8)\times \dfrac{(\mathrm{F}_1\cdot \mathrm{R}\cdot \mathrm{X}_{\mathrm{i}} + \mathrm{F}_2\cdot(1-\mathrm{R})\cdot Puma_{male})}{(2\cdot \mathrm{rand}_9 - 1 + \mathrm{randn}_2)} - \mathrm{Puma}_{\mathrm{male}} & \text{Otherwise} \end{cases} \quad (39)$$

$$round\left(1+\left(N_{pop}-1\right)\cdot rand_{10}\right) \quad (40)$$

$$R = 2\cdot rand_{11} - 1 \quad (41)$$

$$F_1 = randn_3 \cdot \exp\left(2 - Iter\cdot\left(\frac{2}{MaxIter}\right)\right) \quad (42)$$

$$F_2 = w\times (v)^2\cdot \cos\left((2\times rand_{12})\cdot w\right) \quad (43)$$

$$w = randn_4 \quad (44)$$

$$v = randn_5 \quad (45)$$

**Algorithm II** Pseudo-code of the PO exploitation phase

for (each Puma ($X_i$)) do
    Calculate R, $F_1$ and $F_2$ by Eqs. (41), (42) and (43) respectively
    Produce $NewX_i$ by Eq. (39)
    Calculate the cost of $NewX_i$
    if NewX$_i$$Cost$ $< X_i Cost$
        $X_i = NewX_i$
    end
end

Eventually, at the conclusion of this stage, freshly generated solutions are substituted if they have less FF than the present one. A full summary of PO algorithm is shown in its pseudo-code in Algorithm-III and its flowchart in Figure 7.

**Algorithm III** Pseudo-code of the PO Algorithm

% PO Setting
Inputs: The population size N and the maximum number of iterations and parameter settings
Outputs: Puma's location and fitness potential

% Initialization
Create a random population using $X_i$ (i = 1, 2, ..., N).
Calculate Puma's fitness levels.
% Unexperienced Phase
for *Iter = 1 : 3*
    Apply exploration phase (algorithm I)
    Apply exploitation phase (algorithm II )
end
Apply Unexperienced Phase
% Experienced Phase
for *Iter = 4: Max iteration*
    Apply experienced Phase
    if $\text{Score}_{\text{Explore}} > \text{Score}_{\text{Exploit}}$
        % Exploration
        Apply exploration phase (algorithm I)
        if Exploration $NewBestX_i Cost < Puma_{male}\ Cost$
            $Puma_{male} = NewBestX_i$
        end
    else
        % Exploitation
        Apply exploitation phase (algorithm II)
        if Exploitation $NewBestX_i Cost < Puma_{male}\ Cost$
            $Puma_{male} = NewBestX_i$

        end
    end
    % Calculation of functions values
    Update $T$ , $f_1$ , $f_2$ and $f_3$
    Update $Score_{Explore}$ and $Score_{Exploit}$ by Eq. (25)
end

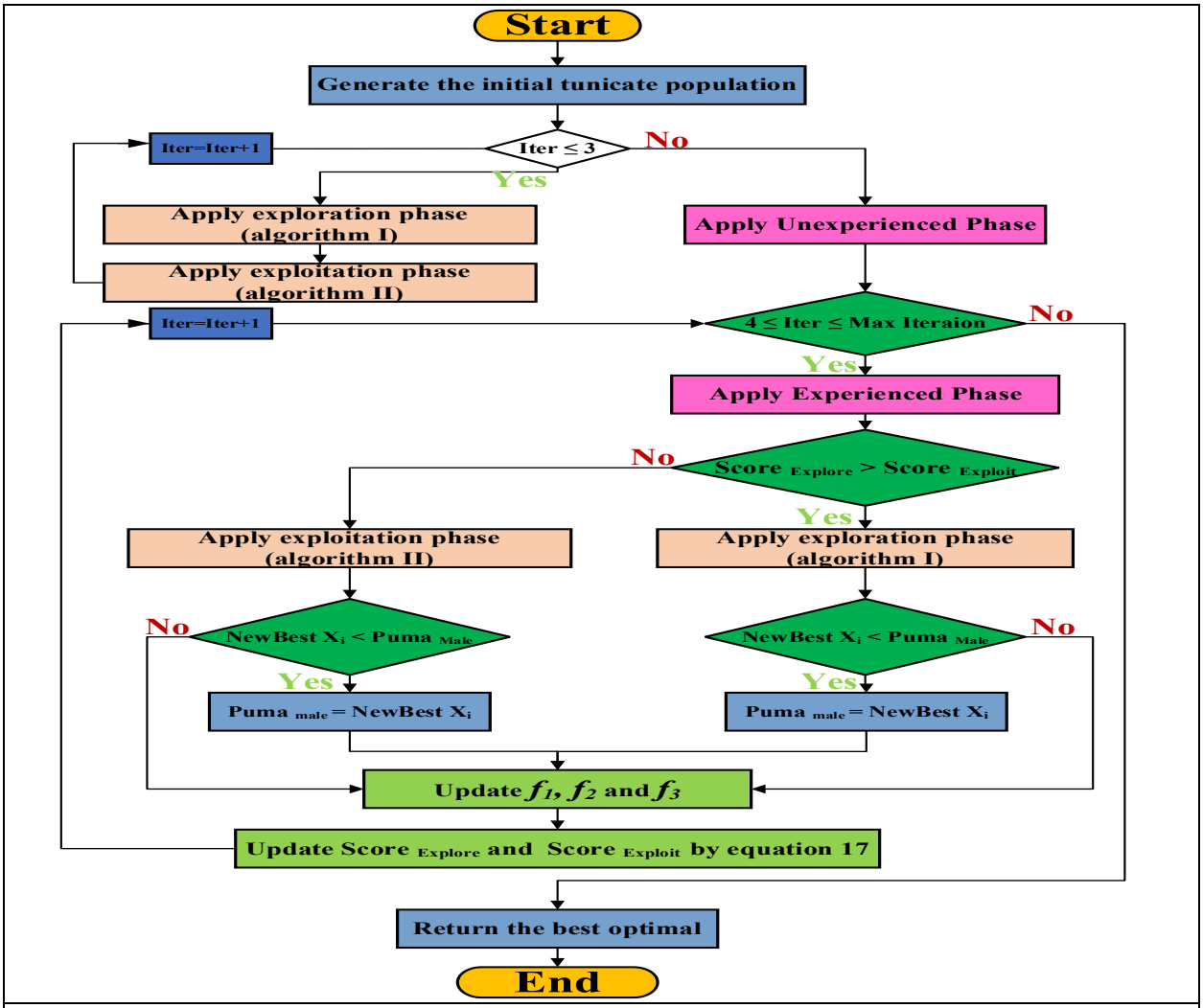



**Figure 7.** Flowchart of PO algorithm.

### *3.4. Computational complexity*

PO is tough to implement but has minimal computational overhead, which varies by phase. The PO's computational challenge involves three processes: initialization, fitness assessment, and solution generation. The computational complexity of each process is summarized in Table 3

**Table 3** The computational complexity of each phase in PO.

| Operation phase | Computational Complexity |
|---|---|
| Initialization | $O(N)$ |
| Exploration | $O\big((2T+1)N^2 \times N \times D\big)$ |
| Exploitation | $O(N \times (T + T \times D))$ |

where N is the overall population number. T is number of iterations. D is number of parameters to be found.

## 4. Numerical scenarios and test cases

This section illustrates various scenarios to demonstrate the proposed controller applied on the suggested system illustrated earlier. Due to RERs' penetration, the effective inertia constant, regulation constant, and frequency bias factor are modified as shown in Eqs. (46)-(48) [49].

$$H_{i,new} = H_{i,old}(1 + P_r - P_c) \quad (46)$$

$$R_{i,new} = \frac{R_{i,old}}{(1 + P_r - P_c)} \quad (47)$$

$$\beta_{i,new} = \frac{(1 + P_r - P_c)}{R_{i,old}} + D_i \quad (48)$$

where $H_{i,new}$, $R_{i,new}$, $and\ \beta_{i,new}$ are the effective inertia constant, regulation constant, and frequency bias factor of area (i), respectively. $H_{i,old}$ , $R_{i,old}$ , $and\ D_i$ are the equivalent inertia constant, regulation constant, and load damping constant of area (i), respectively. Besides that, $P_r$ represents the portion of inertia provided by RERs as well as $P_c$ represents the portion of rotational inertia decreased from traditional generators owing to the existence of RERs. In addition, RERs were assumed to add zero inertia to the system ($P_r = 0$) for both VSWT and PV. Furthermore, VSWT and PV represent 50% of area-I and 20% of area-II generating power, resulting in $P_c$ assumed to be 0.5 pu for area-I and 0.2 pu for area-II. These scenarios were performed by MATLAB/SIMLINK 2022b. The code of different optimizers is developed to accomplish the customized optimization procedure. Optimization process was performed in scenario-I and the performance of PO was demonstrated in later scenarios by a comparison with new algorithm such as Gorilla Troops Optimization (GTO), Hippopotamus Optimizer (HO) [50], and Walrus Optimization Algorithm (WaOA) [51] algorithms as well as benchmark Genetic Algorithm (GA) [52] under different circumstances of load disturbances and real time variable weather circumstances.

To provide an even comparison, the min/max limits of optimized gains are restricted as follows: $K_p, K_I, and\ K_d$ parameters of PIDN controllers' ∈ [0.2, 4], N parameter of PIDN controllers ∈ [0, 200], pitch angle controller gain $(k_\beta)$ ∈ [10,50], VSWT droop $(R_{wt})$ ∈ [0.1, 0.3] and the time constant of the washout filter $(\tau_w)$ ∈ [1, 30]. In addition, the number of population and iterations were set to be 30 and 100, respectively. The selected min/max boundaries of PIDN are determined after extensive trials and around the specified limits in [18,39].

***4.1 Scenario-I: Optimization of controllers' parameters***

The optimal gains of PIDN controllers as well as $\tau_w$, $R_{wt}$ $and$ $k_\beta$ have been allocated using different optimization algorithms. The design process was performed under a severe system case with +20% step load perturbation (SLP) (+10% per area) at t=0. The different parameters were optimized by employing the minimization of the Integral of the Time multiplied Absolute Error (ITAE) as a FF of the tie-line power deviation and frequency aberrations in both areas, as shown in Eq. (49). The selection of ITAE was owing to its ability to increase system setup time. It also has the characteristics of providing small overshoots. The optimal settings for each parameter obtained from different algorithms are given in Table 4. The convergence curves of the 5 optimization algorithms for 100 iterations are shown in Figure 8.

$$ITAE = \int_0^{T_{sim}} [t \cdot (|\Delta F_1| + |\Delta F_2| + |\Delta P_{tie}|)] \cdot dt \tag{49}$$

Table 5 shows that PO outperformed other optimizers and provided the least ITAE. To validate PO superiority, the other FFs have been computed for further statistical analysis. It is observed that PO granted lower ITAE by 2.621%, 24.879%, 21.337%, and 43.164% than WaOA, HO, GTO, and GA, respectively. In addition, the dynamic responses of the system to such a condition for $\Delta F_1, \Delta F_2, and\ \Delta P_{tie}$ are declared in Figure 9. It is noted that the PO algorithm provided the best dynamic results and lower over-/undershooting than other optimizers. It is observed that PO granted lower $\Delta F_1$ shooting by 56.183%, 25.446%, and 2.582% than WaOA, GTO, and GA, respectively. In addition, PO granted lower $\Delta F_2$ shooting by 19.352%, 15.516%, 9.463%, and 7.076% than WaOA, HOA, GTO, and GA, respectively. Moreover, PO granted lower $\Delta P_{tie}$ shooting by 12.406%, 53.781%, 17.063%, and 35.563% than WaOA, HOA, GTO, and GA, respectively. For further comparison, signal statistics of frequency and tie-line power deviations are depicted in Table 6; the overall conclusion is that PO is the most robust algorithm compared with other optimizers.

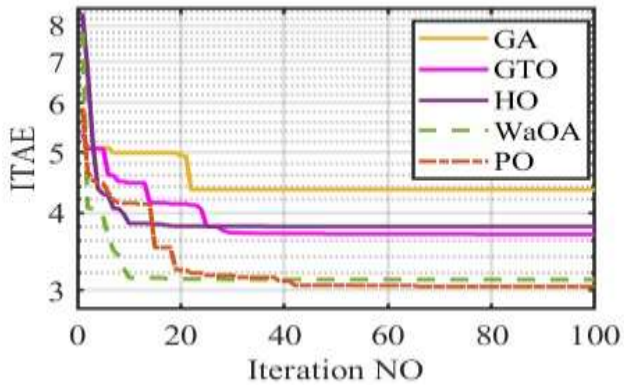



**Figure 8.** Log-scale for convergence curves of different algorithms

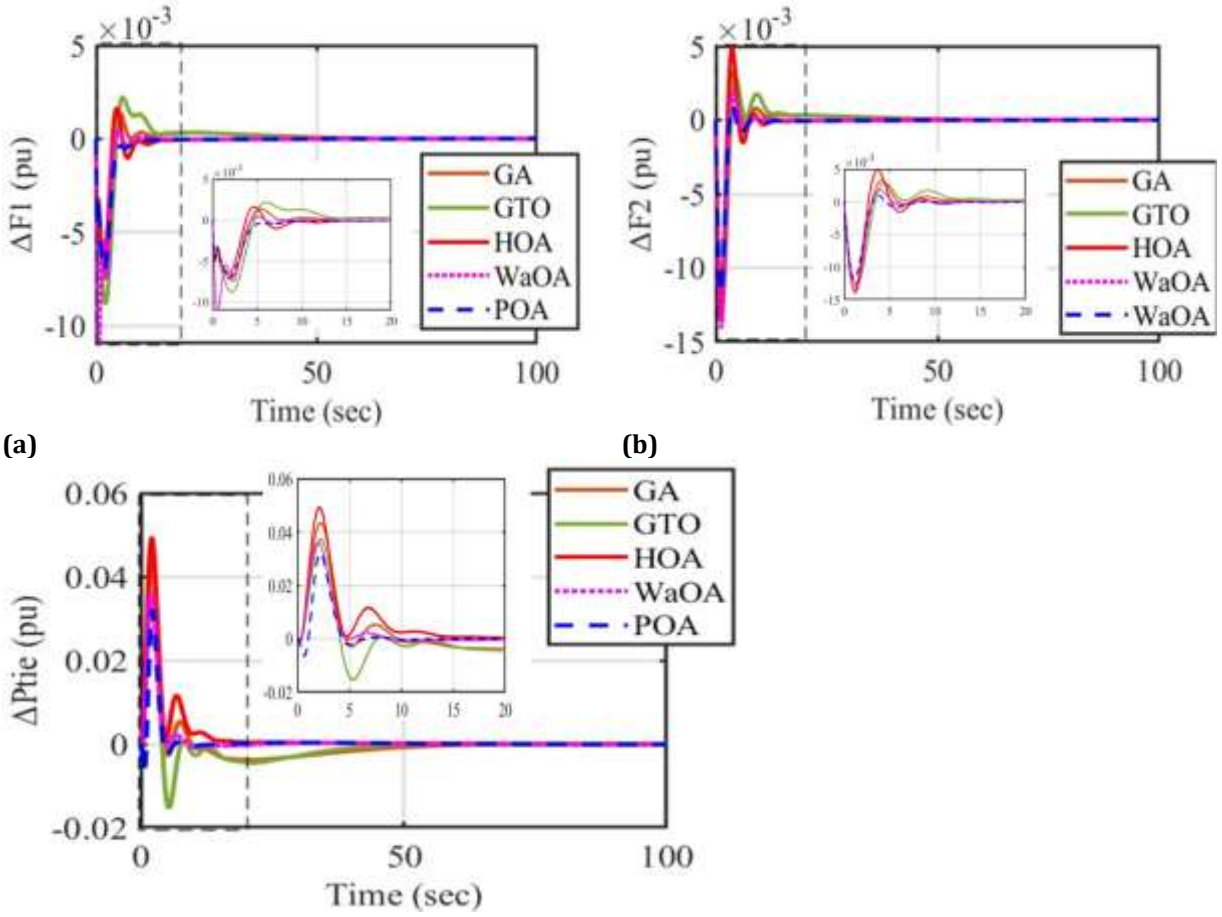



**Figure 9.** Time responses of the system under +20% SLP (+10% for each area) $(a)\Delta F_1$, $(b)\Delta F_2$ *and* $(c)\ \Delta P_{tie}$

**Table 4** PIDN parameters obtained by different algorithms

| | GA | GTO | HO | WaOA | PO |
|---|---|---|---|---|---|
| $k_{p1}$ | 3.4366 | 0.9799 | 4 | 1.6655 | 3.9900 |
| $k_{I1}$ | 1.3742 | 0.7682 | 2.7797 | 0.4677 | 0.5804 |
| $k_{d1}$ | 3.9934 | 4 | 3.1392 | 0.2000 | 3.9999 |
| $N_1$ | 107.5459 | 200 | 127.2787 | 131.9286 | 175.7470 |
| $k_{p2}$ | 3.8490 | 4 | 4 | 4 | 3.9656 |
| $k_{I2}$ | 0.6934 | 0.9104 | 0.2328 | 0.2262 | 0.2222 |
| $k_{d2}$ | 3.6515 | 0.5283 | 1.3256 | 0.3535 | 0.5920 |
| $N_2$ | 111.0147 | 100 | 199.7126 | 200.0000 | 199.9946 |
| $k_{p3}$ | 2.1424 | 2.0512 | 2.2007 | 4 | 3.8639 |
| $k_{I3}$ | 3.7870 | 4 | 3.9960 | 4 | 3.9967 |
| $k_{d3}$ | 1.5424 | 1.6931 | 0.2665 | 0.2 | 0.3218 |
| $N_3$ | 169.0025 | 200 | 126.8256 | 200 | 168.6554 |
| $\tau_W$ | 28.2495 | 30 | 29.9999 | 30 | 29.9959 |
| $k_\beta$ | 49.9847 | 50 | 49.9998 | 50 | 49.9885 |
| $R_{wt}$ | 0.1687 | 0.1 | 0.1167 | 0.100310 | 0.2580 |

**Table 5** Different fitness functions obtained by different algorithms

| OPT | | | | FF | Rank |
|---|---|---|---|---|---|
| | IAE | ISE | ITSE | ITAE | |

| | | | | | |
|---|---|---|---|---|---|
| **GA** | 0.294510 | 0.004034 | 0.015894 | 4.357949 | 5 |
| **GTO** | 0.300215 | 0.003464 | 0.015089 | 3.693523 | 3 |
| **HO** | 0.242922 | 0.004725 | 0.012138 | 3.801350 | 4 |
| **WaOA** | 0.164539 | 0.002481 | 0.005409 | 3.123803 | 2 |
| **PO** | **0.147319** | **0.001800** | **0.004061** | **3.044025** | **1** |

**Table 6** Quality specifications of system responses using different algorithms

| **OPT** | $\Delta F_1$ | | | | $\Delta F_2$ | | | | $\Delta P_{tie}$ | | |
|---|---|---|---|---|---|---|---|---|---|---|---|
| | **MPOS (pu)× $10^{-3}$** | **MNUS (pu)× $10^{-3}$** | $T_s$ **(sec)** | | **MPOS (pu)× $10^{-3}$** | **MNUS (pu)× $10^{-2}$** | $T_s$ **(sec)** | | **MPOS (pu)× $10^{-2}$** | **MNUS (pu)× $10^{-3}$** | $T_s$ **(sec)** |
| **GA** | 1.404 | −7.192 | 65.447 | | 3.301 | −1.256 | 63.282 | | 4.338 | −0.3870 | 65.447 |
| **GTO** | 2.215 | −8.795 | 81.602 | | 2.968 | −1.284 | 79.770 | | 3.746 | −1.526 | 83.435 |
| **HO** | 1.611 | −6.540 | 149.665 | | 4.893 | −1.355 | 146.841 | | 4.921 | −0.09581 | 155.313 |
| **WaOA** | 0.4642 | −10.95 | 54.177 | | 1.817 | −1.400 | 52.129 | | 3.597 | −0.08446 | 55.086 |
| **PO** | 0.480 | −7.011 | 52.379 | | 0.9353 | −1.173 | 49.865 | | 3.200 | −0.6332 | 53.097 |

### *4.2 Scenario II: Robustness of PO under RLP in both areas*

The performance of PO needs more demonstration, so Random Load Perturbations (RLPs) as shown in Figure 10 are applied in both areas and the system dynamic responses are given in Figure 11. It is observed that ITAE for PO was 124.992 pu.sec and less than WaOA, HO, GA, WHO and GTO by 16.009%, 25.842%, 35.219%, and 63.110% respectively. RLPs are divided in 5 sub-scenarios or sections (Figure 10). The statistics of frequency and tie line power deviations as well as percentage reduction in max deviations of PO over other algorithms in the 5 sections are given in Table 7. The percentage reduction is calculated as a percentage of the absolute maximum deviation (MPOS or MNUS) of corresponding PO value to other algorithms in each section as shown in Eq. (50). It is observed that PO gives the lowest value in 52 out of 60 compared results and subsequentially the best performance and demonstrates its resilience and potential as a good, benchmarked algorithm. PO is validated in the next scenario in real weather circumstances.

$$\%\, Reduction = \frac{|Max\ deviation_{other}| - |Max\ deviation_{PO}|}{|Max\ deviation_{PO}|} \times 100 \tag{50}$$

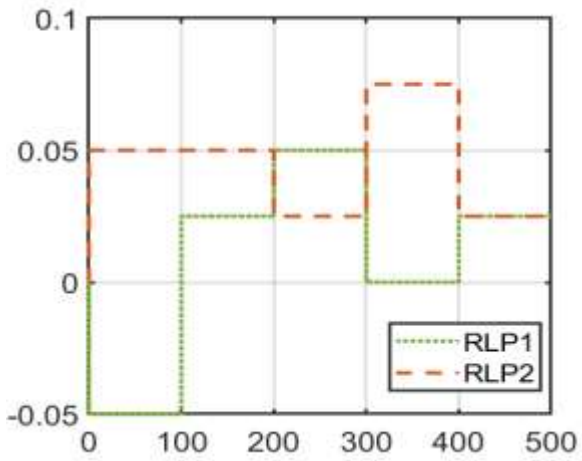
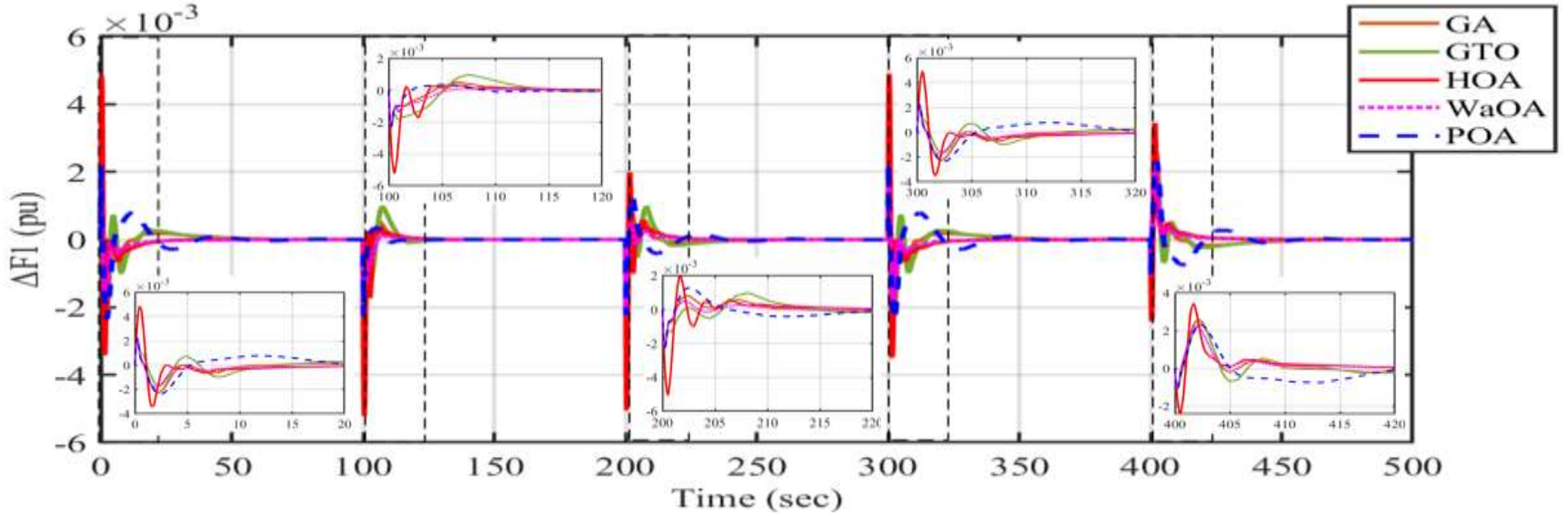
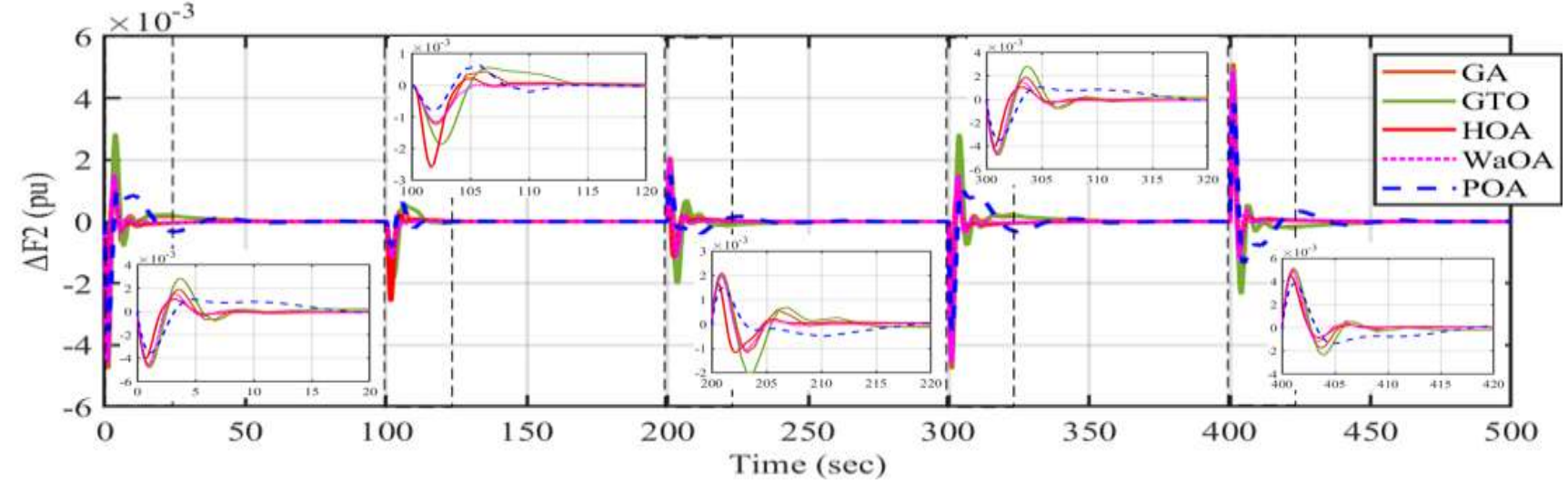


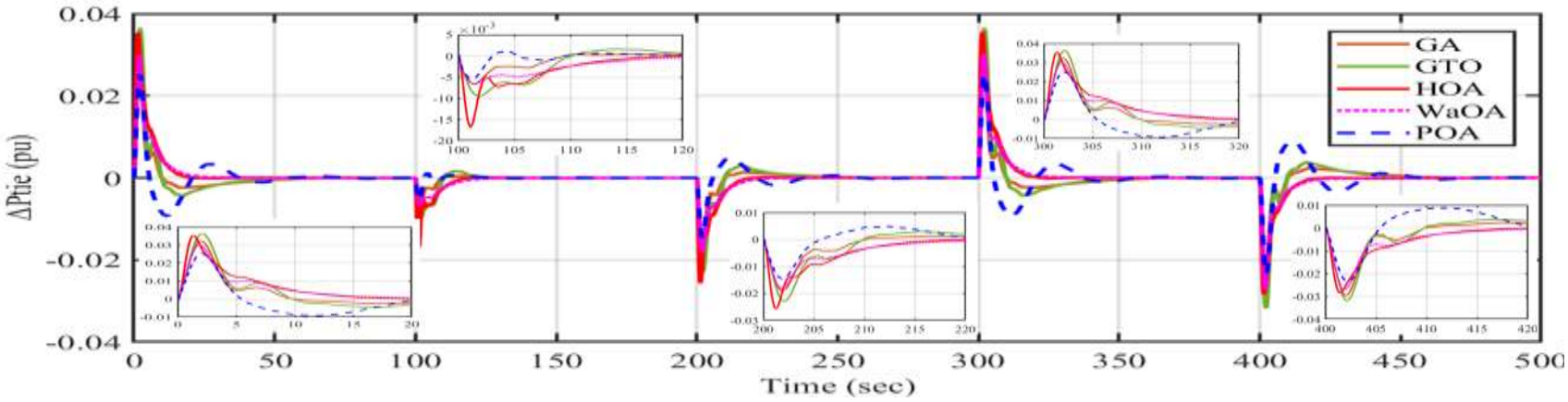

**Figure 10.** RLP subjected to the system at both areas in pu


×10^-3
ΔF1 (pu)
Time (sec)
GA
GTO
HOA
WaOA
POA

**(a)**


×10^-3
ΔF2 (pu)
Time (sec)
GA
GTO
HOA
WaOA
POA

**(b)**




**(c)**

**Figure 11.** Time responses of the system under RLP at both areas area $(a)\Delta F_1$, $(b)\Delta F_2$ *and* $(c)\ \Delta P_{tie}$

**Table 7** Reductions in quality specification $\Delta F_1$, $\Delta F_2$ and $\Delta P_{tie}$ due to 5-sections RLP using PO

| OPT | $\Delta F_1$ | | | | $\Delta F_2$ | | | | $\Delta P_{tie}$ | | |
|---|---|---|---|---|---|---|---|---|---|---|---|
| | MPOS (pu)$\times 10^{-3}$ | MNUS (pu)$\times 10^{-3}$ | Reduction (%) | | MPOS (pu)$\times 10^{-3}$ | MNUS (pu)$\times 10^{-3}$ | Reduction (%) | | MPOS (pu)$\times 10^{-2}$ | MNUS (pu)$\times 10^{-3}$ | Reduction (%) |
| | | | | | | | | | | | |
| **Section 1** | | | | | | | | | | | |
| **-5% on area-I & +5% on area-II** | | | | | | | | | | | |
| **GA** | 2.258 | −2.308 | 5.436 | | 1.887 | −4.789 | 4.586 | | 3.227 | −2.319 | 7.854 |
| **GTO** | 2.243 | −1.675 | 2.467 | | 2.834 | −4.597 | 0.393 | | 3.637 | −4.422 | 21.557 |
| **HO** | 2.456 | −2.705 | 23.752 | | 1.916 | −5.250 | 14.654 | | 3.157 | −5.047 | 5.515 |
| **WaOA** | 4.892 | −3.460 | 123.48 | | 1.056 | −3.993 | ___ | | 3.533 | −1.407 | 18.082 |
| **PO** | 2.189 | −1.797 | ___ | | 1.499 | −4.579 | ___ | | 2.992 | −3.278 | ___ |
| | | | | | | | | | | | |
| **Section 2** | | | | | | | | | | | |
| **+2.5% on area-I & +5% on area-II** | | | | | | | | | | | |
| **GA** | 0.5225 | −2.338 | 3.819 | | 0.4800 | −1.241 | 5.527 | | 0.04157 | −6.547 | ___ |
| **GTO** | 0.9622 | −2.311 | 2.620 | | 0.5562 | −1.850 | 57.313 | | 0.1640 | −9.541 | 44.912 |
| **HO** | 0.5741 | −2.522 | 11.989 | | 0.7517 | −1.147 | ___ | | 0.05966 | −6.161 | ___ |
| **WaOA** | 0.4091 | −5.198 | 130.817 | | 0.2404 | −2.594 | 120.578 | | 0 | −16.77 | 154.708 |
| **PO** | 0.1074 | −2.252 | ___ | | 0.02535 | −1.176 | ___ | | 0 | −6.584 | ___ |
| | | | | | | | | | | | |
| **Section 3** | | | | | | | | | | | |

| | | | | | | | | | | | |
|---|---|---|---|---|---|---|---|---|---|---|---|
| **+5% on area-I & +2.5% on area-II** | | | | | | | | | | | |
| **GA** | 0.8339 | −2.298 | 2.635 | | 2.088 | −1.170 | 4.192 | | 0.1325 | −19.05 | 5.191 |
| **GTO** | 0.9725 | −2.287 | 2.144 | | 1.961 | −2.069 | 3.244 | | 0.3002 | −23.02 | 27.112 |
| **HO** | 1.263 | −2.497 | 11.523 | | 2.301 | −0.9604 | 14.820 | | 0 | −18.08 | __ |
| **WaOA** | 1.983 | −5.043 | 125.234 | | 1.676 | −1.140 | __ | | 0.01574 | −25.57 | 41.193 |
| **PO** | 0.4778 | −2.239 | __ | | 2.004 | −1.127 | __ | | 0 | −18.11 | __ |
| | | | | | | | | | | | |
| **Section 4** | | | | | | | | | | | |
| **+0% on area-I & +7.5% on area-II** | | | | | | | | | | | |
| **GA** | 2.235 | −2.260 | 3.527 | | 1.893 | −4.768 | 4.128 | | 3.224 | −2.354 | 7.503 |
| **GTO** | 2.258 | −1.670 | 3.436 | | 2.835 | −4.598 | 0.415 | | 3.637 | −4.481 | 21.274 |
| **HO** | 2.459 | −2.710 | 24.141 | | 1.918 | −5.252 | 14.698 | | 3.167 | 0.04798 | 5.602 |
| **WaOA** | 4.861 | −3.461 | 122.675 | | 1.040 | −4.009 | __ | | 3.543 | −0.1183 | 18.139 |
| **PO** | 2.183 | −1.790 | __ | | 1.479 | −4.579 | __ | | 2.999 | 0 | __ |
| | | | | | | | | | | | |
| **Section 5** | | | | | | | | | | | |
| **+2.5% on area-I & +2.5% on area-II** | | | | | | | | | | | |
| **GA** | 2.573 | −1.092 | 15.537 | | 5.125 | −1.747 | 5.714 | | 0.2219*e* | −29.41 | 9.250 |
| **GTO** | 2.367 | −1.119 | 6.286 | | 4.983 | −2.336 | 2.785 | | 0.3774 | −31.69 | 17.719 |
| **HO** | 2.829 | −1.198 | 27.032 | | 5.611 | −1.972 | 15.738 | | 0 | −29.60 | 9.955 |
| **WaOA** | 3.436 | −2.405 | 54.288 | | 4.491 | −0.8764 | __ | | 0.0006921 | −28.2 | 5.089 |
| **PO** | 2.227 | −1.070 | __ | | 4.848 | −1.183 | __ | | 0.004199 | −26.92 | __ |

***4.3 Scenario-III: Performance of PO under real variable weather circumstances***

Actual data at Zafarana in Egypt, for irradiance, temperature and wind speed are used to verify the PO performance incorporating the PIDN controller. Figure 12 shows four-day of irradiance, temperature, and wind speed samples. In addition, the system reactions, $\Delta F_1, \Delta F_2$ *and* $\Delta P_{tie}$ , as a result of actual weather data are shown in Figure 13. For the DAPS, the highest frequency variation is −0.002225 pu (−0.1112 Hz). Which is a safe number based on the function of the under-frequency load shedding relays [1,53,54]. Therefore, it is evident that the system functions adequately under actual atmospheric circumstances.

In summary of the performance of PO and from the optimization results of PIDN controllers, we see that PO gives the best fitness function. PO also shows its robustness under random stiff load disturbances in the 2nd scenario, while it also behaves satisfactorily in real weather conditions in the 3rd scenario. In the studied cases, PO behaves better than other optimizers. This is because PO has different hunting strategies in the jungle. The random movement helps to explore the search space, while the algorithm has immunity to being stuck in local minima by updating the new score, as described by Eq. (25).

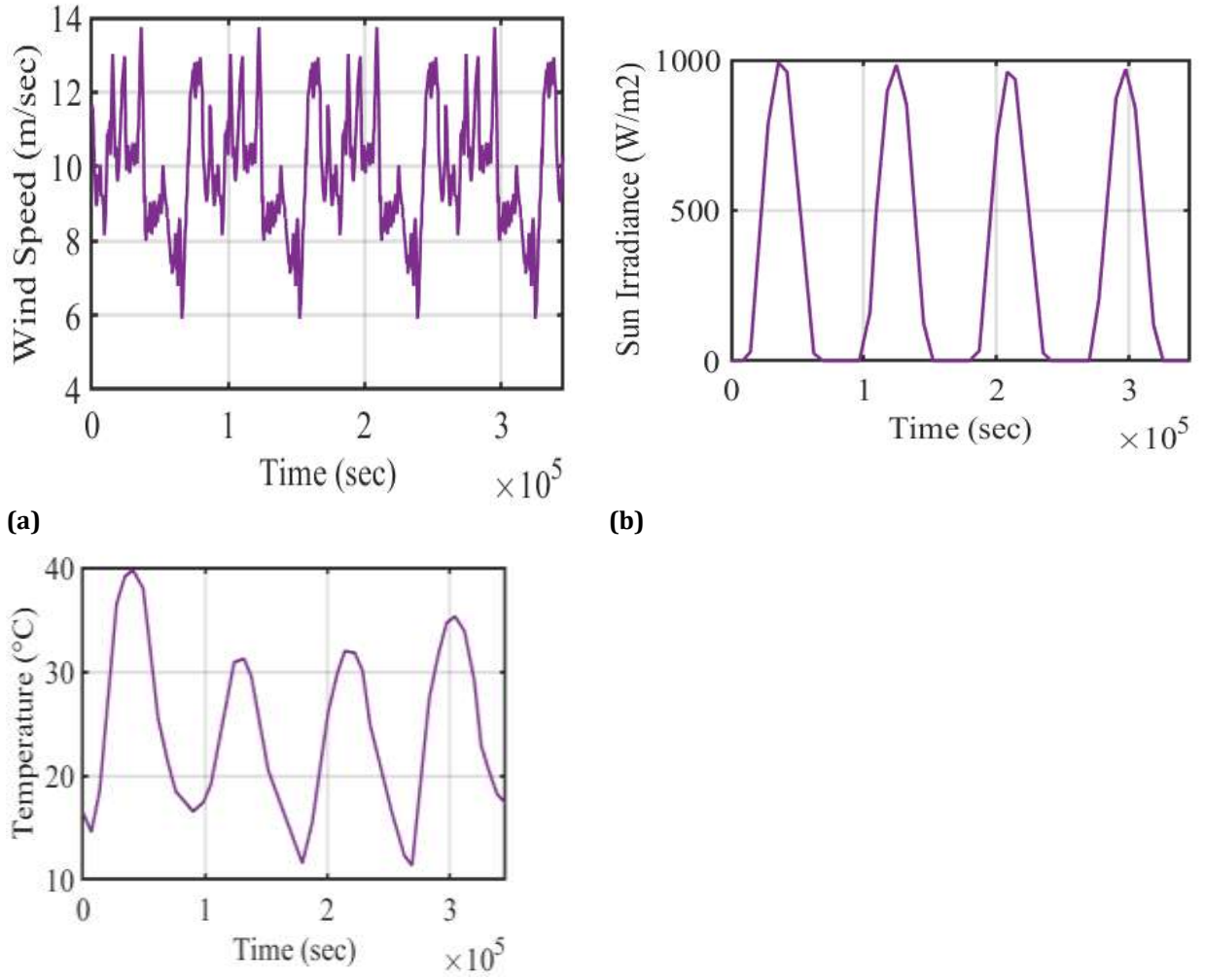



**Figure 12.** Real variable weather circumstances (a) Wind Speed, (b) Sun irradiance, and (c) Temperature

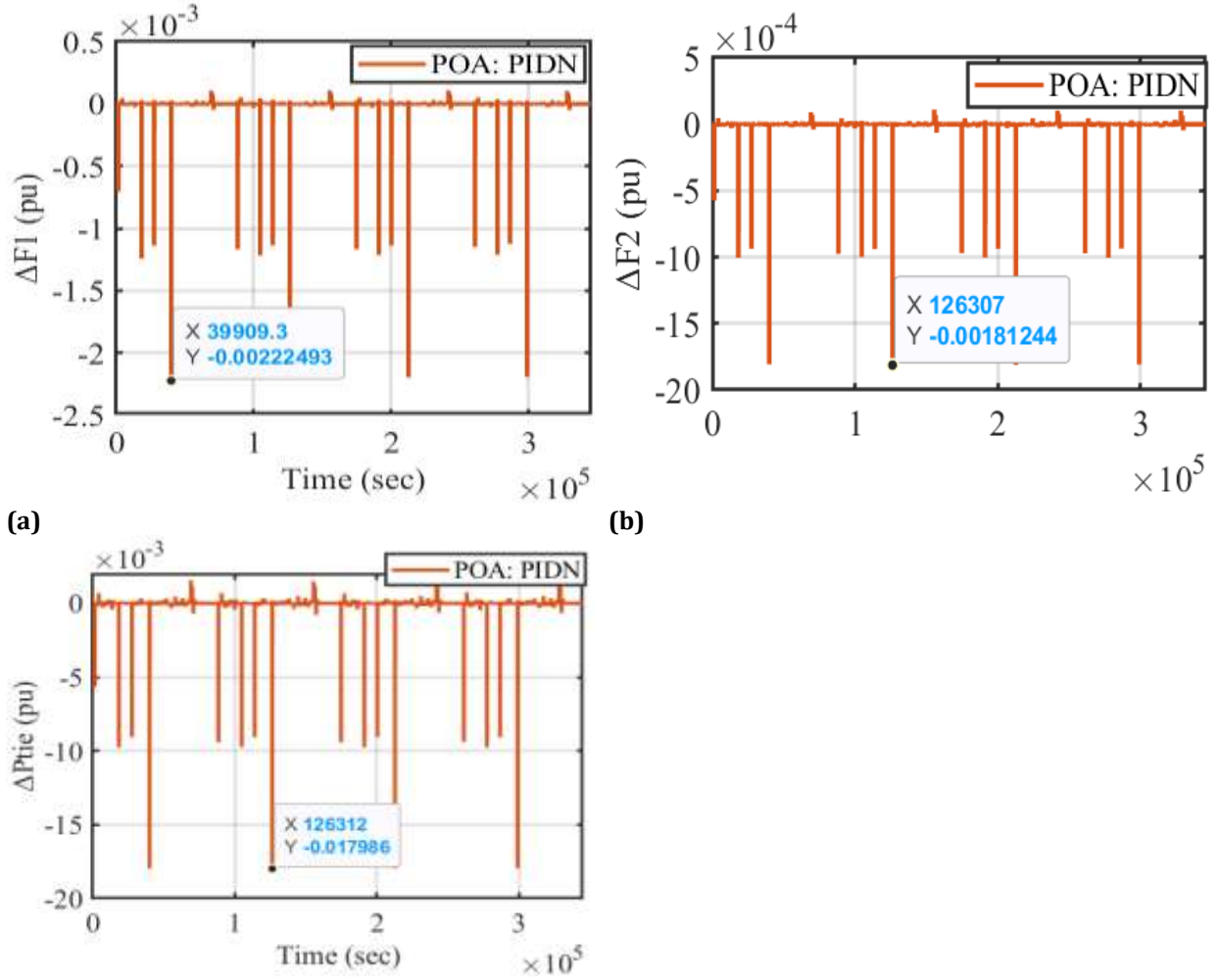



**Figure 13.** Time responses of the system under actual weather data

## 5. Conclusion

In this paper, an efficient LFC has been performed on a DAPS using robust PIDN, pitch angle, droop, and auxiliary storage controllers. This DAPS comprises hydro and steam generators combined with a high penetration of RERs such as wind turbine generator and PV panels. The optimal parameters which satisfy the best value of ITAE are obtained by the PO, HO, GTO, WaOA, and GA approaches. The efficacy and validity of the PO is validated through three scenarios with comparisons to other benchmarked optimizers. Optimization is first performed with +20% SLP (+10% at each area) and the results confirm that the PO results are the best. It is observed that PO granted lower ITAE by 2.621%, 24.879%, 21.337%, and 43.164% than WaOA, HO, GTO, and GA, respectively. It is noted that the PO algorithm provided the best dynamic results and lower over-/undershooting than other optimizers. It is observed that PO granted lower $\Delta F_1$ by 56.183%, 25.446%, and 2.582% than WaOA, GTO, and GA, respectively. In addition, PO granted lower $\Delta F_2$ by 19.352%, 15.516%, 9.463%, and 7.076% than WaOA, HOA, GTO, and GA, respectively. Moreover, PO granted lower $\Delta P_{tie}$ by 12.406%, 53.781%, 17.063%, and 35.563% than WaOA, HOA, GTO, and GA, respectively. In the 2nd scenario, the system was studied under RLP where RLPs are divided into 5 sub-scenarios or sections. Finally, the performance evaluation of PIDN optimized by the PO is examined in real weather conditions. This results in a maximum frequency deviation of −0.002225 pu which is safe according to underfrequency relay operation. The results illustrate the applicability and efficiency of the proposed PIDN controllers based on the PO approach.

**Statements and Declarations**

**Informed consent statement**

The study did not involve humans.

**Disclosure statement**

The authors have no relevant conflict of interest to disclose.

**Data availability statement**

Data sets generated during the current study are available from the corresponding author on reasonable request.

**Funding**

The authors declare that no funds, grants, or other support were received during the preparation of this manuscript.

**Authors contributions statement**

**Abdelfattah M. Elmoaty**: Conceptualization, Methodology, Software, Writing—Original draft preparation, Data curation. **Ahmed M. Othman**: Visualization, Investigation, Writing—Reviewing and Editing. **Mahdi M. Elarini**: Writing— Reviewing and Editing, Supervision.

All authors have participated in (a)drafting the article or revising it critically for important intellectual content; and (b) approval of the final version.

## References

[1] Hussain J, Zou R, Pathak PK, Karni A, Akhtar S. Design of a novel cascade PI-(1+FOPID) controller to enhance load frequency control performance in diverse electric power systems. Electr Power Syst Res. 2025;243:111488. doi:10.1016/j.epsr.2025.111488.

[2] Singh A, Yadav S, Tiwari N, Nishad DK, Khalid S. Optimized PID controller and model order reduction of reheated turbine for load frequency control using teaching learning-based optimization. Sci Rep. 2025;15:3759. doi:10.1038/s41598-025-87866-z.

[3] Veerendar T, Kumar D. Teaching-learning optimizer-based FO-PID for load frequency control of interlinked power systems. Int J Model Simul. 2023;43:683–705. doi:10.1080/02286203.2022.2112009.

[4] Lamba R, Singla SK, Sondhi S. Design of Fractional Order PID Controller for Load Frequency Control in Perturbed Two Area Interconnected System. Electr Power Components Syst. 2019;47:998–1011. doi:10.1080/15325008.2019.1660736.

[5] Singh VP, Kishor N, Samuel P. Improved load frequency control of power system using LMI based PID approach. J Franklin Inst. 2017;354:6805–30. doi:10.1016/j.jfranklin.2017.08.031.

[6] Guha D, Roy PK, Banerjee S. Grasshopper optimization algorithm scaled fractional order PI-D controller applied to reduced order model of load frequency control system. Int J Model Simul. 2020;40:217–42. doi:10.1080/02286203.2019.1596727.

[7] Guha D, Roy PK, Banerjee S. Quasi-oppositional JAYA optimized 2-degree-of-freedom PID controller for load-frequency control of interconnected power systems. Int J Model Simul. 2022;42:63–85. doi:10.1080/02286203.2020.1829444.

[8] Gulzar MM, Iqbal M, Shahzad S, Muqeet HA, Shahzad M, Hussain MM. Load Frequency Control (LFC) Strategies in Renewable Energy-Based Hybrid Power Systems: A Review. Energies. 2022;15. doi:10.3390/en15103488.

[9] El-Rifaie AM. A Novel Lyrebird Optimization Algorithm for Enhanced Generation Rate-Constrained Load Frequency Control in Multi-Area Power Systems with Proportional Integral Derivative Controllers. Processes. 2025;13. doi:10.3390/pr13040949.

[10] Sonker B, Kumar D, Samuel P. Design of two degree of freedom-internal model control configuration for load frequency control using model approximation. Int J Model Simul. 2019;39:27–37. doi:10.1080/02286203.2018.1474027.

[11] Goyal H, Handmandlu M, Kothari DP. A Novel Modelling Technique for Automatic Load Frequency Control of Small Hydro Power Plants. Int J Model Simul. 2007;27:186–92. doi:10.1080/02286203.2007.11442416.

[12] Liu X, Shi K, Zhou K, Wen S, Tang Y, Tang L. Event-triggering-based H∞ load frequency control for multi-area cyber–physical power system under DoS attacks. Franklin Open. 2023;3:100012. doi:10.1016/j.fraope.2023.100012.

[13] Tuan DH, Tran DT, Nguyen Ngoc Thanh V, Huynh V V. Load Frequency Control Based on Gray Wolf Optimizer Algorithm for Modern Power Systems. Energies. 2025;18. doi:10.3390/en18040815.

[14] D R, G MK. Artificial Raindrop Algorithm-Based Load Frequency Control in PV-Thermal-Thermal Interconnected Power System. Electr Power Components Syst. 2023:1–11. doi:10.1080/15325008.2023.2261125.

[15] Chi X, Liu X, Jia X. Multi-rate sampled-data observer-based networked load frequency control for multi-

area interconnected power systems under multiple cyber-attacks. J Franklin Inst. 2025;362:107427. doi:10.1016/j.jfranklin.2024.107427.

[16] Thorat R, Bhatt P. Electric vehicle participation for optimized load frequency control in a multi-area restructured power system. Int J Model Simul. 2024:1–14. doi:10.1080/02286203.2024.2327640.

[17] Khokhar B, Parmar KPS. Load frequency control performance enhancement of an electric vehicle integrated time-delay multi-microgrid system. Int J Model Simul. 2024:1–18. doi:10.1080/02286203.2024.2392223.

[18] El-Hameed MA, Elkholy MM, El-Fergany AA. Efficient frequency regulation in highly penetrated power systems by renewable energy sources using stochastic fractal optimiser. IET Renew Power Gener. 2019;13:2174–83. doi:10.1049/iet-rpg.2019.0186.

[19] Ma T, Barajas-Solano DA, Tartakovsky AM. Chance constrained load frequency control of power systems with wind resources. J Franklin Inst. 2025;362:107478. doi:10.1016/j.jfranklin.2024.107478.

[20] Kumar R, Sikander A. A new hybrid approach based on fuzzy logic and optimization for load frequency control. Int J Model Simul. 2024:1–10. doi:10.1080/02286203.2024.2315327.

[21] Dokht Shakibjoo A, Moradzadeh M, Moussavi SZ, Mohammadzadeh A, Vandevelde L. Load frequency control for multi-area power systems: A new type-2 fuzzy approach based on Levenberg–Marquardt algorithm. ISA Trans. 2022;121:40–52. doi:10.1016/j.isatra.2021.03.044.

[22] Cui M, Zhao Y, Cao P, Tang Y, Lu Y. Load frequency control of interconnected hydrothermal power system based on FOPI + FOPD controller. Int J Dyn Control. 2024;12:1073–85. doi:10.1007/s40435-023-01212-7.

[23] Arora K, Kumar A, Kamboj VK, Prashar D, Shrestha B, Joshi GP. Impact of Renewable Energy Sources into Multi Area Multi-Source Load Frequency Control of Interrelated Power System. Mathematics. 2021;9. doi:10.3390/math9020186.

[24] Xie Y, Liao P, Liang Z, Zhou D. State of Change-Related Hybrid Energy Storage System Integration in Fuzzy Sliding Mode Load Frequency Control Power System with Electric Vehicles. Machines. 2025;13. doi:10.3390/machines13010057.

[25] Nayak PC, Umesh Chandra P, Ramesh Chandra P, and Panda S. Imperialist competitive algorithm optimized cascade controller for load frequency control of multi-microgrid system. Energy Sources, Part A Recover Util Environ Eff. 2025;47:5538–60. doi:10.1080/15567036.2021.1897710.

[26] Khadanga RK, Kumar A, Panda S. A novel modified whale optimization algorithm for load frequency controller design of a two-area power system composing of PV grid and thermal generator. Neural Comput Appl. 2020;32:8205–16. doi:10.1007/s00521-019-04321-7.

[27] Guha D, Roy PK, Banerjee S. Whale optimization algorithm applied to load frequency control of a mixed power system considering nonlinearities and PLL dynamics. Energy Syst. 2020;11:699–728. doi:10.1007/s12667-019-00326-2.

[28] Çelik E. Improved stochastic fractal search algorithm and modified cost function for automatic generation control of interconnected electric power systems. Eng Appl Artif Intell. 2020;88:103407. doi:10.1016/j.engappai.2019.103407.

[29] Kumar B, Adhikari S, Datta S, Sinha N. Real time simulation for load frequency control of multisource microgrid system using grey wolf optimization based modified bias coefficient diagram method (GWO-MBCDM) controller. J Electr Eng Technol. 2021;16:205–21. doi:10.1007/s42835-020-00596-2.

[30] Veerendar T, Kumar D, Kumar Gupta A. Quasi-Oppositional African Vultures Optimization-Based PIλDn Plus PIλ Controller for Frequency Control of an Interlinked Hybrid Power System. Electr Power Components Syst. 2023:1–21. doi:10.1080/15325008.2023.2191249.

[31] Persson M, Chen P. Frequency control by variable speed wind turbines in islanded power systems with various generation mix. IET Renew Power Gener. 2017;11:1101–9. doi:10.1049/iet-rpg.2016.0350.

[32] Varzaneh SG, Abedi M, Gharehpetian GB. A new simplified model for assessment of power variation of DFIG-based wind farm participating in frequency control system. Electr Power Syst Res. 2017;148:220–9. doi:10.1016/j.epsr.2017.03.033.

[33] Bhagat SK, Saikia LC, Babu NR. Application of artificial hummingbird algorithm in a renewable energy source integrated multi-area power system considering Fuzzy based tilt integral derivative controller. E-Prime-Advances Electr Eng Electron Energy. 2023;4:100153. doi:10.1016/j.prime.2023.100153.

[34] Siti MW, Mbungu NT, Tungadio DH, Banza BB, Ngoma L. Application of load frequency control method to a multi-microgrid with energy storage system. J Energy Storage. 2022;52:104629. doi:10.1016/j.est.2022.104629.

[35] Saadatinezhad H, Ramezani A, Alizadeh M, Hajimalek E. Fault tolerant load frequency sharing of a multi-

area power system using model predictive control. J Eng. 2022;2022:337–47. doi:10.1049/tje2.12117.
[36] Alahakoon S, Roy RB, Arachchillage SJ. Optimizing Load Frequency Control in Standalone Marine Microgrids Using Meta-Heuristic Techniques. Energies. 2023;16:4846. doi:10.3390/en16134846.
[37] Mishra DK, Mohanty A, Ray PK. An optimal frequency regulation in interconnected power system through differential evolution and firefly algorithm. Soft Comput. 2024;28:593–606. doi:10.1007/s00500-023-08314-6.
[38] Krishna PJ, Meena VP, Patnana N, Mathur A, Singh VP. Grey wolf optimizer-assisted R-method-based weighted minimization for automatic generation control in two-area interconnected power system. Int J Dyn Control. 2023;11:1779–96. doi:10.1007/s40435-022-01070-9.
[39] El-Bahay MH, Lotfy ME, El-Hameed MA. Effective participation of wind turbines in frequency control of a two-area power system using coot optimization. Prot Control Mod Power Syst. 2023;8:1–15. doi:10.1186/s41601-023-00289-8.
[40] Clark K, Miller NW, Sanchez-Gasca JJ. Modeling of GE wind turbine-generators for grid studies. vol. 4.5. 4.5. General Electric International, Inc. New York, NY, USA; 2010.
[41] Ghani F, Rosengarten G, Duke M, Carson JK. The numerical calculation of single-diode solar-cell modelling parameters. Renew Energy. 2014;72:105–12. doi:10.1016/j.renene.2014.06.035.
[42] Ali EE, El-Hameed MA, El-Fergany AA, El-Arini MM. Parameter extraction of photovoltaic generating units using multi-verse optimizer. Sustain Energy Technol Assessments. 2016;17:68–76. doi:10.1016/j.seta.2016.08.004.
[43] De Soto W, Klein SA, Beckman WA. Improvement and validation of a model for photovoltaic array performance. Sol Energy. 2006;80:78–88. doi:10.1016/j.solener.2005.06.010.
[44] El-Fergany A. Efficient Tool to Characterize Photovoltaic Generating Systems Using Mine Blast Algorithm. Electr Power Components Syst. 2015;43:890–901. doi:10.1080/15325008.2015.1014579.
[45] K. Arthishri, R. Balasubramanian, Parkavi Kathirvelu SPS and RA. Maximum Power Point Tracking of Photovoltaic Generation System using Artificial Neural Network with Improved Tracking Factor. J Appl Sci. 2014;14:1858–64. doi:10.3923/jas.2014.1858.1864.
[46] Kundur, P. S., Malik OP. Power system stability and control. USA: Mc-Graw Hill Education; 2022.
[47] Abdollahzadeh B, Khodadadi N, Barshandeh S, Trojovský P, Gharehchopogh FS, El-kenawy E-SM, Abualigah L, Mirjalili S. Puma optimizer (PO): A novel metaheuristic optimization algorithm and its application in machine learning. Cluster Comput. 2024:1–49. doi:10.1007/s10586-023-04221-5.
[48] Andic C, Ozturk A, Aydin E, Turkay B. A Novel Puma Optimizer Based TID Controller for Load Frequency Control. 2024 Glob. Energy Conf., 2024, p. 1–6. doi:10.1109/GEC61857.2024.10881981.
[49] Nguyen N, Pandit D, Quigley R, Mitra J. Frequency Response in the Presence of Renewable Generation: Challenges and Opportunities. IEEE Open Access J Power Energy. 2021;8:543–56. doi:10.1109/OAJPE.2021.3118393.
[50] Amiri MH, Mehrabi Hashjin N, Montazeri M, Mirjalili S, Khodadadi N. Hippopotamus optimization algorithm: a novel nature-inspired optimization algorithm. Sci Rep. 2024;14:5032. doi:10.1038/s41598-024-54910-3.
[51] Hussain J, Zou R, Wu Z, Pathak PK, Akhtar S. Design and Performance Analysis of Walrus Optimization Algorithm (WaOA)-Based Cascade Controller for Load Frequency Control of a Multi-Area Power System With Renewable Sources. Int J Numer Model Electron Networks, Devices Fields. 2025;38:e70046. doi:10.1002/jnm.70046.
[52] Huang Z, Chen Z, Zheng Y, Sun M, Sun Q. Optimal design of load frequency active disturbance rejection control via double-chains quantum genetic algorithm. Neural Comput Appl. 2021;33:3325–3345. doi:10.1007/s00521-020-05199-6.
[53] Commission IE. IEC TS 62786 Distributed Energy Resources Connection with the Grid. Int Electrotech Comm Geneva, Switz. 2023.
[54] Committee PSR. Ieee guide for the application of protective relays used for abnormal frequency load shedding and restoration. IEEE Std C. 2007;37:c1–43. doi:10.1109/IEEESTD.2007.4299516.